THE FIVE-MINUTE OSCILLATIONS - WHAT'S LEFT TO BE DONE

Edward J. Rhodes, Jr.
Department of Astronomy and Earth and Space Sciences Institute
University of Southern California
Los Angeles, CA 90007

Roger K. Ulrich
Department of Astronomy
University of California at Los Angeles
Los Angeles, CA 90024

John W. Harvey
Kitt Peak National Observatory
Tucson, Arizona 85717

Thomas L. Duvall, Jr.
NASA Southwestern Station
Kitt Peak National Observatory
Tucson, Arizona 85717

ABSTRACT

A brief review is given of the observational and theoretical progress made since the discovery of the solar "5-minute" oscillations by Leighton, Noyes, and Simon (1962). In particular, attention is given to the recent identification of these oscillations as non-radial p-mode, or acoustic, oscillations of the whole sun. Current observational methods for studying these oscillations at large horizontal wavenumbers are discussed in detail and several two-dimensional (k_h-ω) power spectra obtained with a CID camera on the main spectrograph of the McMath telescope at Kitt Peak National Observatory are described. The best-resolved observations of the p-mode yet obtained at chromospheric elevations are also presented. Recent progress in studies of the p-modes at low wavenumbers with full-disk velocity detection schemes is summarized next. These full-disk observations of radial (ℓ = o) and low-degree non-radial ($1 \leq \ell \leq 4$) modes are shown to place severe constraints on the theoretical calculation of solar interior structure. Recent progress in making fully-consistent solar models which fit both the high- and low-wavenumber observations will also be described. Finally, the observational and theoretical improvements that are most necessary for further progress in solar seismology will be summarized.

1. Introduction

The so-called "5-minute" solar oscillations were initially discovered in the late 1950's with the 60-foot tower telescope at Mount Wilson by Leighton, Noyes, and Simon (1962). Initially, these oscillations were thought to be a purely atmospheric phenomenon, in particular, a response of the solar atmosphere to the overshooting of

individual convective granules from below the photosphere. The first observations to show some degree of spatial and temporal structure in these oscillations were those of Frazier (1968). Two wavenumber-frequency (k_h-ω) power spectra computed by Frazier from his observations are illustrated in Figure 1. These spectra were the first to show two strong peaks of oscillatory power near a horizontal wavenumber, $k_h = 2\pi/\lambda$, of 1 Mm^{-1}. As we will see shortly, the locations of these two power peaks have been confirmed by much more highly-resolved power spectra.

Following Frazier's observational evidence for the existence of more than one resonant mode in the 5-minute frequency band, Ulrich published in 1970 the first theoretical explanation of these 5-minute oscillations as non-radial, standing acoustic waves which were trapped in a resonant cavity located below the solar photosphere (Ulrich, 1970). In this paper Ulrich went on to make predictions of the locations in wavenumber and frequency of the strongest observational power based on one solar model and pointed out that only Frazier's earlier study was at all sensitive to these modes.

The first observations to go beyond the identification of the two isolated power peaks seen in Figure 1 and suggest the reality of Ulrich's (1970) predictions were those of Franz Deubner (1975). Deubner's results, obtained in 1974 at Capri, showed a hint of the ridge structure first predicted by Ulrich; however, the observational ridges were not sharply defined and their disagreement in frequency with Ulrich's detailed predictions was apparent.

Working independently of Deubner, George Simon, Roger Ulrich, and Edward Rhodes began a study of the 5-minute oscillations late in 1974 here at Sacramento Peak Observatory using the 512-channel diode array on the Tower Telescope. The results from this study, which were published subsequently to Deubner's (1975) results, showed beyond doubt that the 5-minute oscillations are truly non-radial p-modes, as Ulrich has originally predicted (Rhodes, Ulrich, and Simon, 1977a). The principal (k_h-ω) power spectrum obtained by Rhodes, Ulrich, and Simon is shown here as Figure 2. The contour diagram shows the distinct observational ridges, while the theoretical p-mode eigenfrequencies calculated by Ulrich and Rhodes (1977) for two different model solar envelopes are superimposed as the two sets of solid curves.

The calculation of the model solar envelopes used to compute the theoretical frequencies shown in Figure 2 is illustrated schematically in Figure 3. This figure shows that the model solar envelopes were computed with a computer code which only integrates inward from the low corona or chromosphere to a finite depth below the photosphere. The solar radius was matched in these calculations, however, the solar luminosity was not even calculated since the models did not extend inward to the region of maximum energy generation in the solar core. The model envelope code was used because it alone treated the radiative transport properties of the atmosphere in sufficient detail for computation of the non-adiabatic

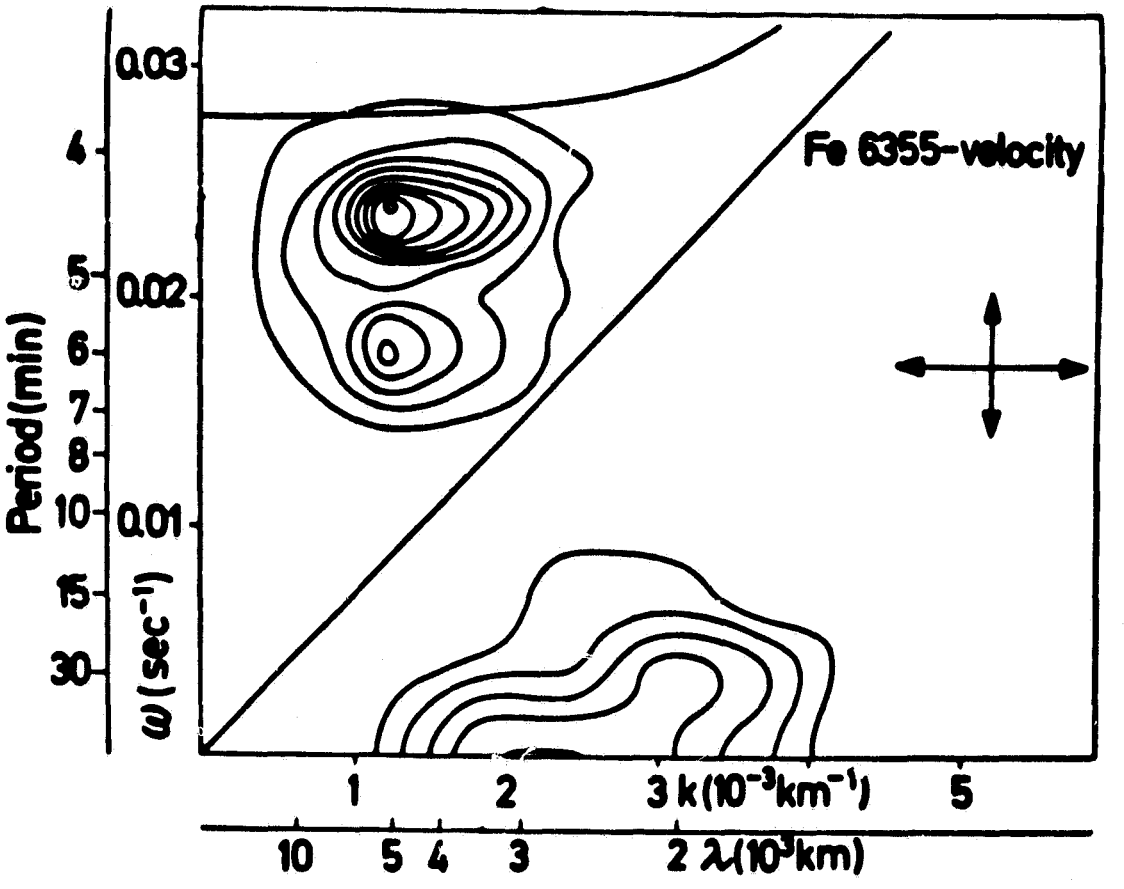
Fe 6355-velocity
Period (min)
ω (sec⁻¹)
0.03
0.02
0.01
4
5
6
7
8
10
15
30
1
2
3 k(10⁻³km⁻¹)
5
10
5
4
3
2 λ(10³km)

a

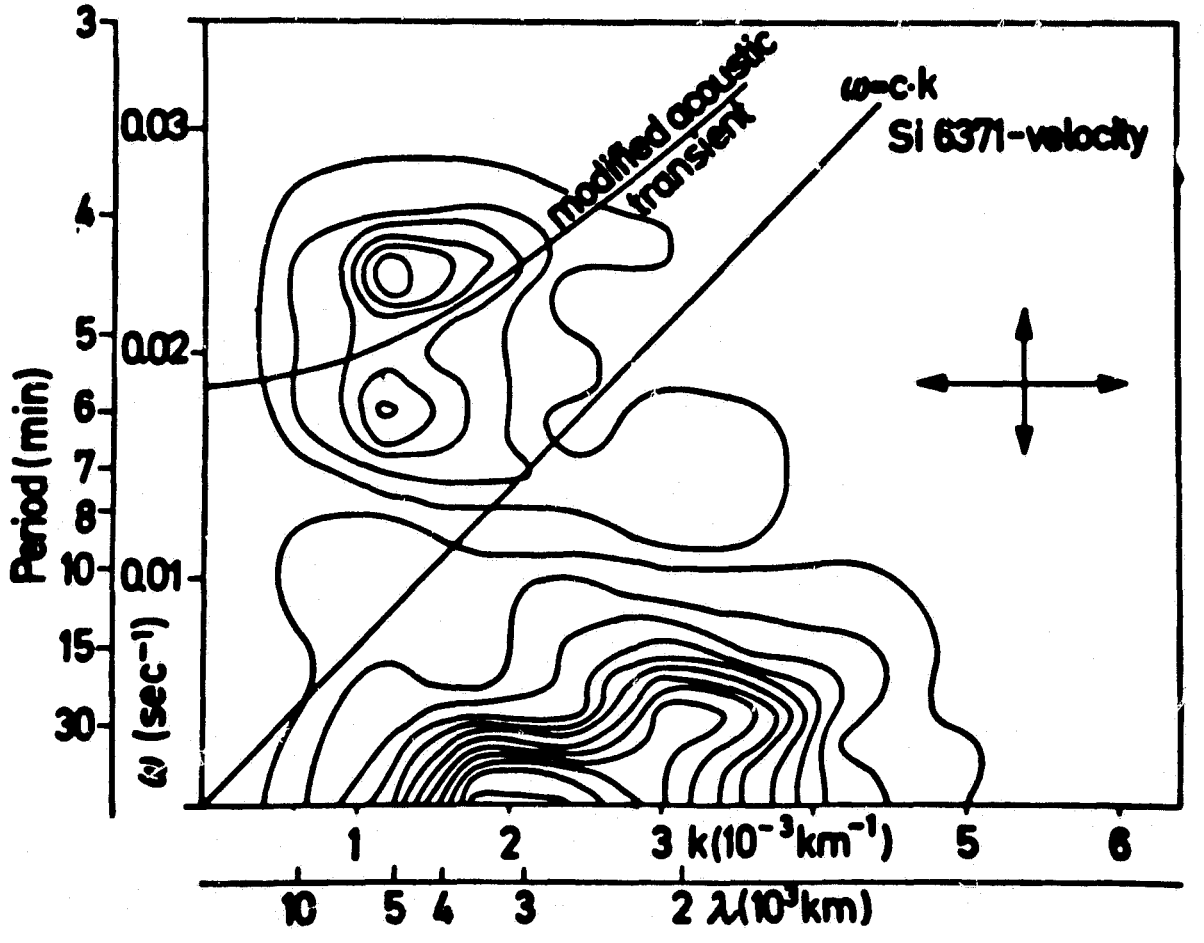
ω=c·k
Si 6371-velocity
modified acoustic transient
Period (min)
ω (sec⁻¹)
3
0.03
4
5
0.02
6
7
8
10
0.01
15
30
1
2
3 k(10⁻³km⁻¹)
5
6
10
5
4
3
2 λ(10³km)

Fig. 1

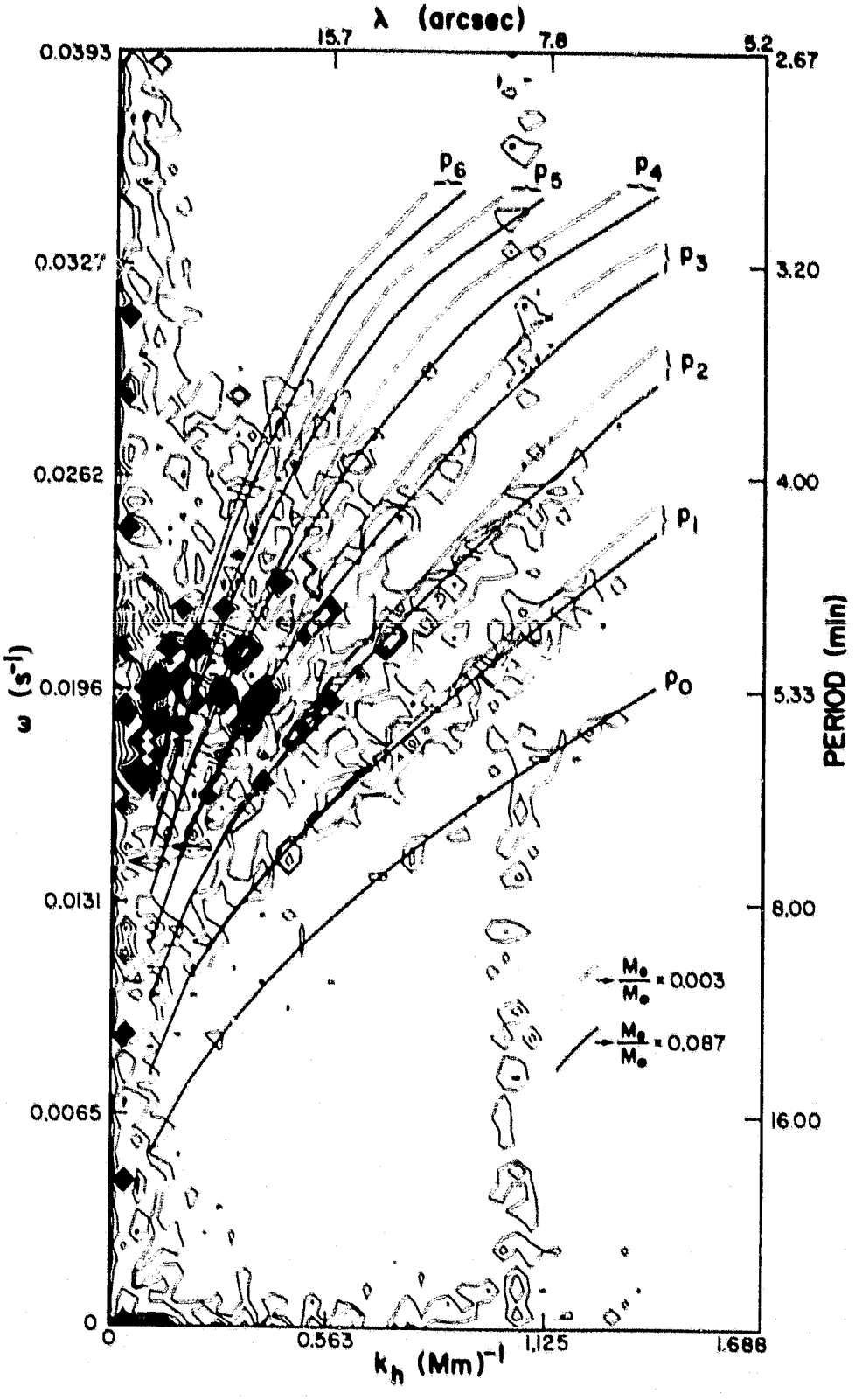
λ (arcsec)
15.7
7.8
5.2
2.67
0.0393
0.0327
0.0262
0.0196
0.0131
0.0065
0
ν (s⁻¹)
p6
p5
p4
p3
p2
p1
p0
3.20
4.00
5.33
8.00
16.00
PERIOD (min)
M0/Me = 0.003
M0/Me = 0.087
0
0.563
1.125
1.688
kh (Mm)⁻¹

Fig. 2

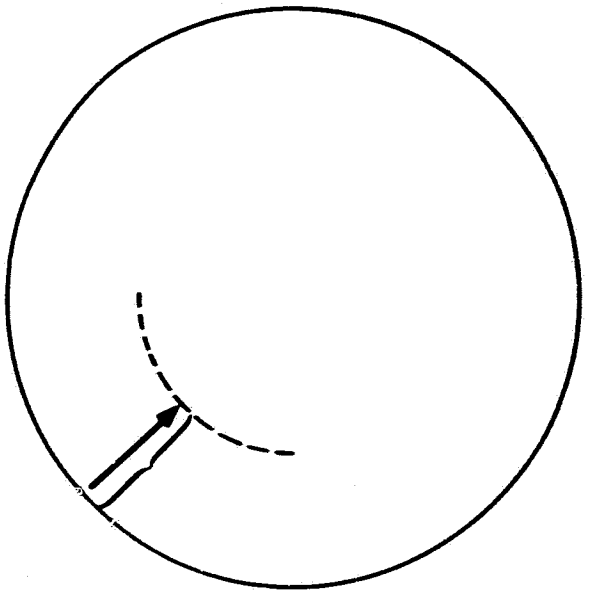

INITIAL ENVELOPE MODELS

- $R_\odot$ CORRECT
- $L_\odot$ NOT COMPUTED
- INWARD INTEGRATION, BUT NOT ALL THE WAY TO CENTER
- DIFFERENT ℓ/H VALUES ARE INPUT TO GET DIFFERENT CONVECTION ZONE DEPTHS

Fig. 3

eigenmodes. Furthermore, the fact that the model envelopes did not extend inward to the center of the sun meant that different convective mixing length to pressure scale height ratios, ℓ/H, could be used to generate different model envelopes in order to study the sensitivity of the p-mode eigenfrequencies to convection zone thickness, as was done by Ulrich and Rhodes (1977) and displayed in Figure 2. The two different sets of curves displayed in Figure 2 correspond to two different ℓ/H ratios, and hence to two different convection zone thicknesses. The upper set of curves corresponds to $\ell/H = 1.2$, while the lower set corresponds to $\ell/H = 3.0$.

Next, Franz Deubner also obtained observations here at Sacramento Peak. These observations, obtained in 1977, are displayed in Figure 4, which is a modification of figure 2 of Deubner, Ulrich, and Rhodes (1979). This figure shows considerable improvement in the observational resolution of the individual p-mode ridges. It also shows two slightly different sets of theoretical eigenfrequencies. Both sets of frequencies correspond ℓ/H ratios equal to 2.0. The upper, or dashed curves correspond to the theory as published in Ulrich and Rhodes (1977), while the lower, or solid, curves are those published by Lubow, Rhodes, and Ulrich (1980). In these calculations a corona was added to the model atmosphere, an outgoing wave outer boundary replaced the earlier zero boundary condition, and Coulomb corrections were made in the equation of state. The effect of all of these improvements was a slight lowering of the p-mode eigenfrequencies which removed the previous small discrepancy between the dashed ridges and Deubner's observations. This figure represents the level of accuracy available one and one-half years ago in the comparison between theory and observation.

2. Current Observational Status

2.1 High Wavenumber Modes

The horizontal wavenumber, k_h, is equal to $\sqrt{\ell(\ell+1)}\,/R_\odot$, where ℓ is the spherical harmonic degree of the particular mode, or the number of wavelengths of the mode contained around the solar circumference. Thus, k_h is approximately linearly proportional to ℓ, and the wavenumber scale of the k_h-ω diagrams is really a spherical harmonic degree scale.

The well-resolved portions of Figures 2 and 4 correspond approximately to ℓ values greater than 150 to 200. It is this portion of the k_h-ω plane which Jack Harvey, Tom Duvall, and I have been studying for the past two years with a CID camera attached to the main spectrograph of the McMath telescope at Kitt Peak National Observatory, as I will illustrate in the next several figures.

First, we concentrate on a $300''$ x $992''$ rectangle centered on the solar disk as illustrated in Figure 5. In this arrangement the spectrograph entrance slit is located in the east-west direction at disk center. A rapidly-rotating prism block is then used to optically average the sunlight over the $300''$ north-south direction onto the entrance slit. In this way

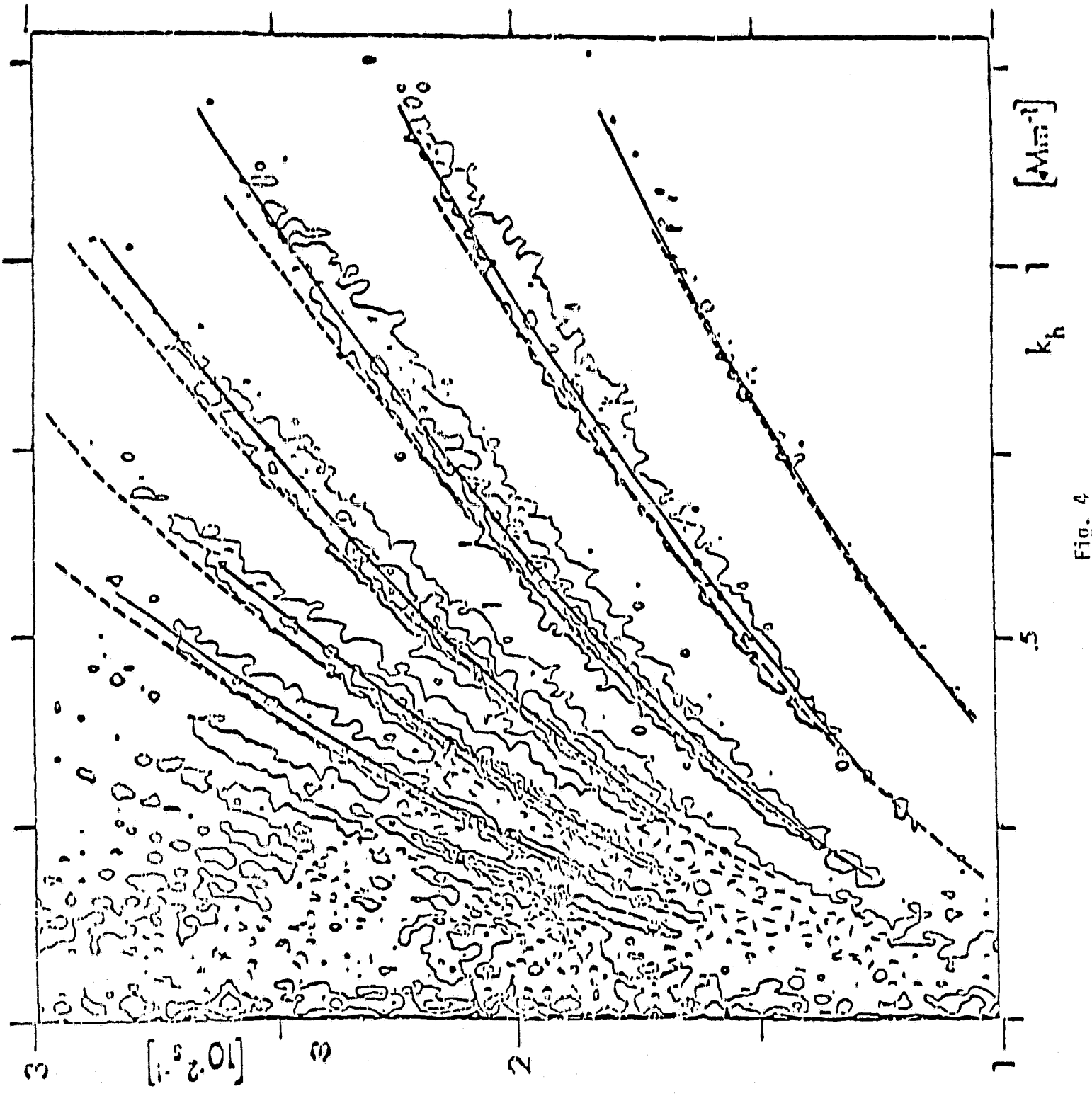

Fig. 4

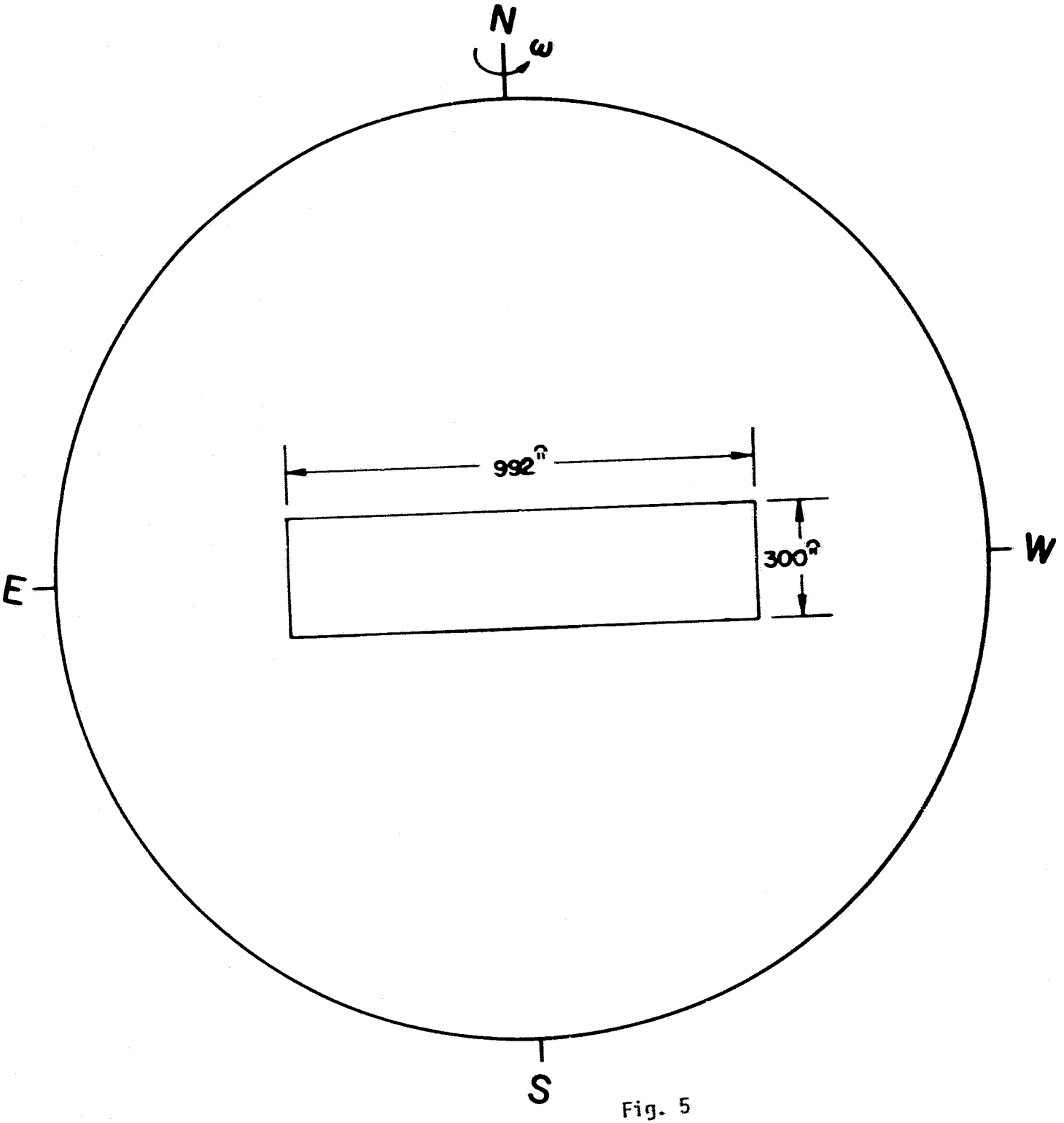

Fig. 5

the CID array camera sees 248 averaged spectra, each covering a region 300" high by 4" wide on the sun. By simultaneously recording on the CID chip a short (~ 2Å wide) segment of the averaged spectrum as seen at each location along the entrance slit, we are able to cover 992" (=248 x 4") in east-west extent as illustrated.

By optically averaging in the north-south direction we are principally looking at sectoral harmonics of different ℓ values, some of which are propagating eastward around the sun and others westward. Most of the obliquely-propagating modes are filtered out except at very low wavenumbers. Sectoral harmonics are sharply peaked at the solar equator, as is illustrated in Figure 6. In this figure the relative amplitudes of three different sectoral harmonics are plotted as three different functions of colatitude angle, θ. All three harmonics sharply peak around the equator ($\theta = 90°$) as described. The ℓ-dependence shows that these harmonics peak more sharply as ℓ increases. Thus, these high-wavenumber p-modes located near the right side of each observational power spectrum are more localized in latitude than are the lower wavenumber modes located nearer the left-hand side of each spectrum.

The equipment setup we currently use at Kitt Peak is shown in Figure 7. In this figure all of our observing equipment is located on top of the round tank of the main Littrow spectrograph. The CID camera dewar is shown at the left, while the guider and prism block assembly are located over the entrance slit on the centerline of the tank. The black enclosure near the CID dewar contains the optical elements which image the resulting spectrum onto the CID chip within the dewar.

We use the four-quadrant guider shown in Figure 7 to keep the solar image centered on the entrance slit and expose the CID seven times during each one-minute scan period for as long as possible each day. In one day we obtain a three-dimensional (x, T, λ) array of numbers, where x is space in the east-west direction, T is time in one-minute samples, and λ covers a short range centered about a single spectral line as indicated. After removal of some image defects and temporal instrumental drifts, the solar line profiles are converted into 248 relative Doppler velocities for each spectral scan. In this way we end up with a two-dimensional space-time (x, T) array of velocities for each observing run.

A sample velocity-space-time diagram which resulted from a single day's observing run is shown in Figure 8. In this figure space runs horizontally while time runs vertically and the velocity at each of the 248 spatial locations has been converted into a grey-lined intensity value. Thus, predominant spatial scales of the oscillations show up as the wave-like ripples which appear to drift in space as time increases downward. This diagonal pattern drift is simply due to the rotation of the sun. The peak-to-peak velocity amplitudes along a single time frame (i.e. along one horizontal row) range up to 30 m/sec, while the noise on a single row is roughly 0.01 that level, or 30 cm/sec.

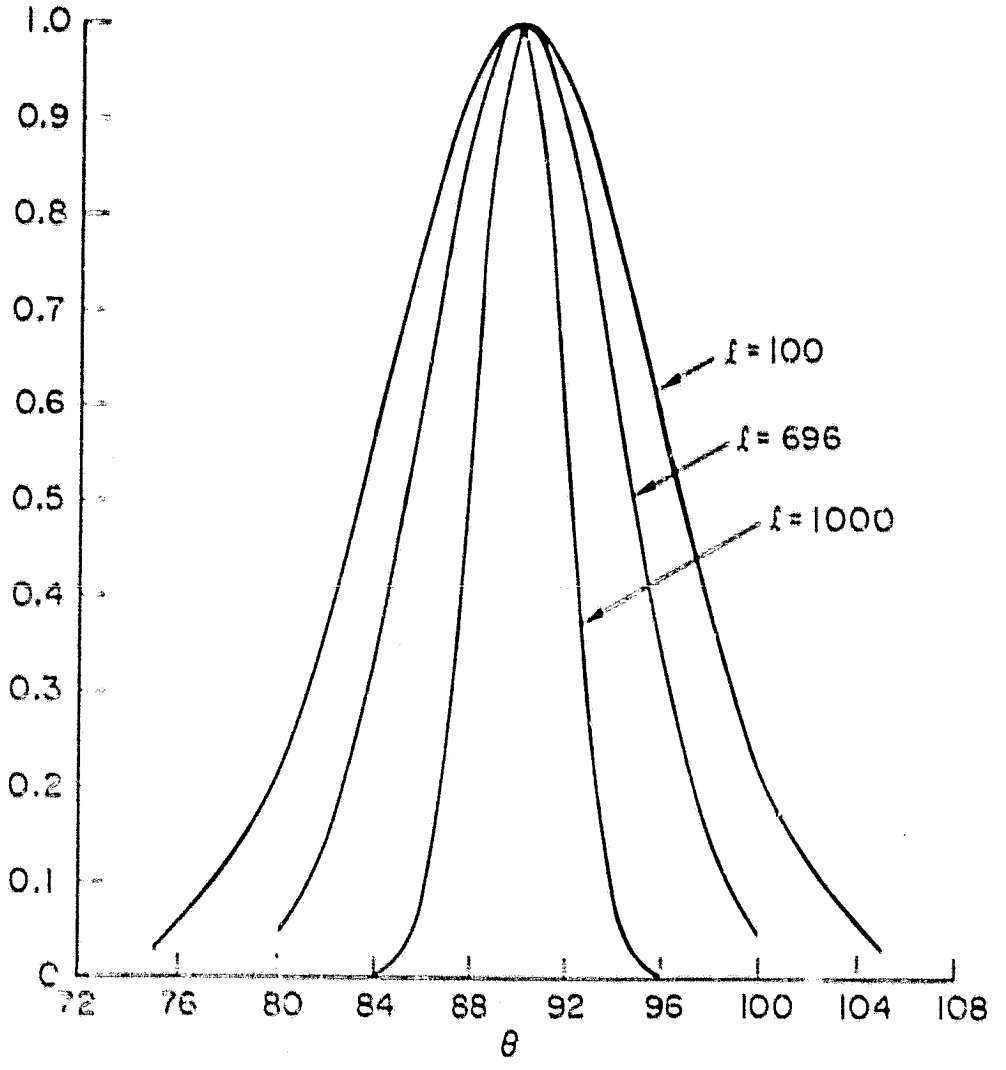
1.0
0.9
0.8
0.7
0.6
0.5
0.4
0.3
0.2
0.1
0
72
76
80
84
88
92
96
100
104
108
θ
f = 100
f = 696
f = 1000

Fig. 6

ORIGINAL PAGE IS
OF POOR QUALITY

FIG. 7

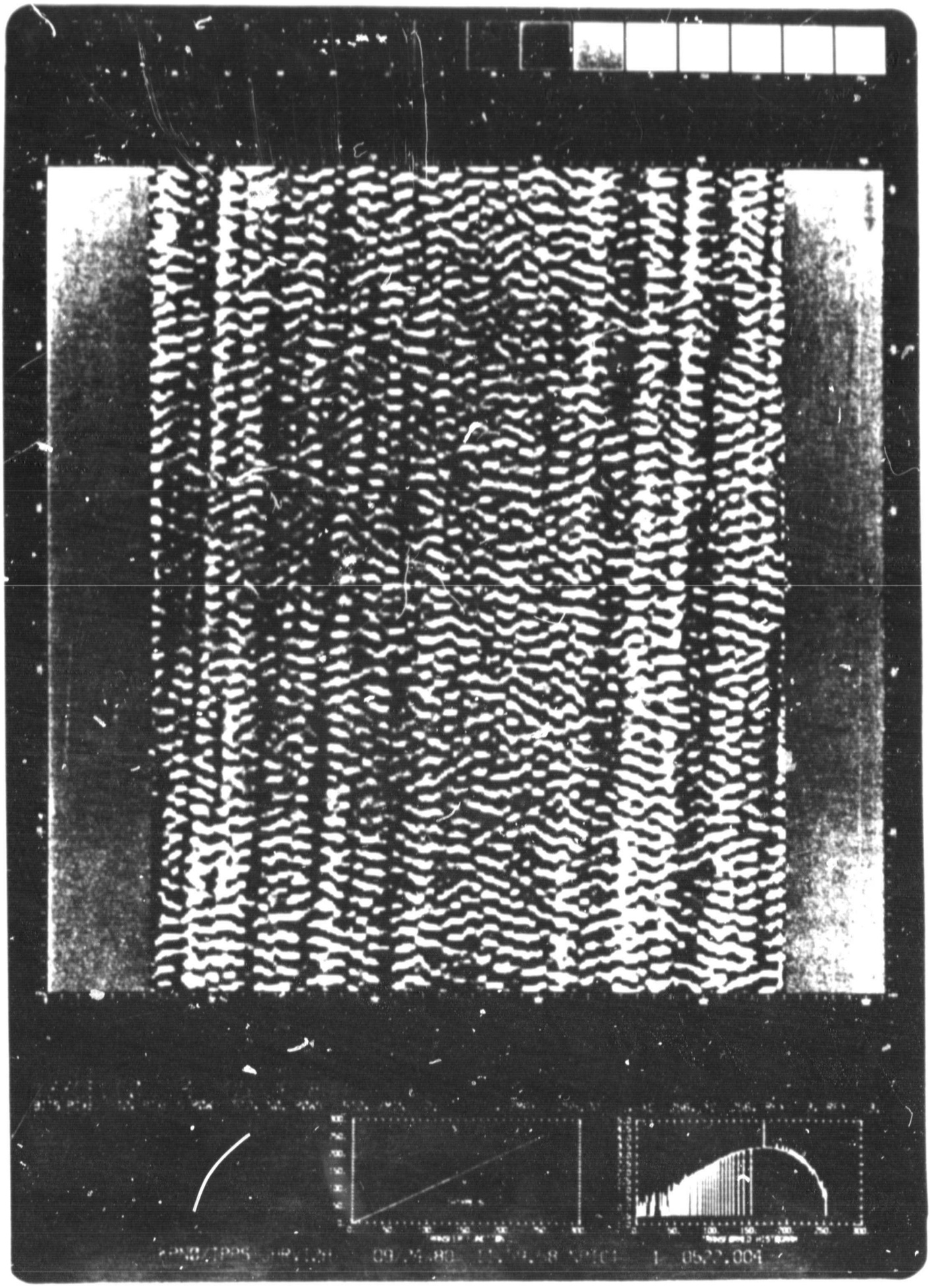

Fig. 2

Whenever possible during each observing run at Kitt Peak, the experimental setup was left unchanged from one day to the next and observations were obtained on as many consecutive days as possible. In this manner observing sequences of up to five days in length were obtained. An example of a k_h-ω power spectrum which resulted from two successive days' of observations is shown in Figure 9. The data from which this spectrum was computed were obtained on May 26 and 27, 1980. Observations were obtained for up to 12 hours on each of these days; however, only one data segment consisting of 512 one-minute frames (having a duration of 8.4 hours) was selected from each day's observations. The two 8.4 hour data strings were Fourier transformed separately and two (k_h-ω) power spectra were obtained. These two spectra were then simply averaged together to obtain the spectrum of Figure 9. The frequency shift introduced in this spectrum by the sun's rotation is visible upon careful inspection. The solar limb positions were recorded and all of the small telescope-guiding drifts were removed from the data prior to the calculation of the two spectra, so that the observed frequency shifts should be solely due to solar rotation.

Even though the frequency shifts can now be measured with better than two percent precision for spectra such as Figure 9, our measurements of the horizontal wavenumber scale must be analyzed in greater detail before we can obtain rotational velocity measurements to that level of accuracy (since $V_{Rot} \approx \Delta\omega/k_h$). In particular, the combined effects of image distortion in the optical system (mainly due to the anamorphic lens used to magnify the spectrum in the direction of the dispersion) and foreshortening of the observing area on the sun must be calibrated and removed before the wavenumber scale can be calculated to one percent on an absolute basis. The effects of the combined distortion and foreshortening on a k_h-ω power spectrum are illustrated qualitatively in Figures 10 and 11. Figure 10 shows the power spectrum obtained from the 8.4-hour run on 26 May 1980 before and after correction for foreshortening and distortion. The original uncorrected spectrum is shown at the right while the corrected spectrum is shown at the left. The most notable difference is the overall sharpening-up of the ridges at intermediate wavenumbers, with the appearance of the fundamental mode (P_o) most altered. Figure 11 shows closeups of the central portions of the corrected and uncorrected spectra shown in Figure 10. The sharpening of the ridges due to the removal of the distortion and foreshortening is shown more clearly here, with the fundamental mode showing up much more obviously in the corrected spectrum. Because the removal of foreshortening also alters the absolute wavenumbers slightly from their uncorrected counterparts, great care must be taken before the corrected wavenumber scale is used in place of the uncorrected scale. This problem is now under intensive study.

In addition to sharpening the observed p-mode ridges, information from multi-day observing runs may shed light on the excitation mechanism

26 to 31 May 1780

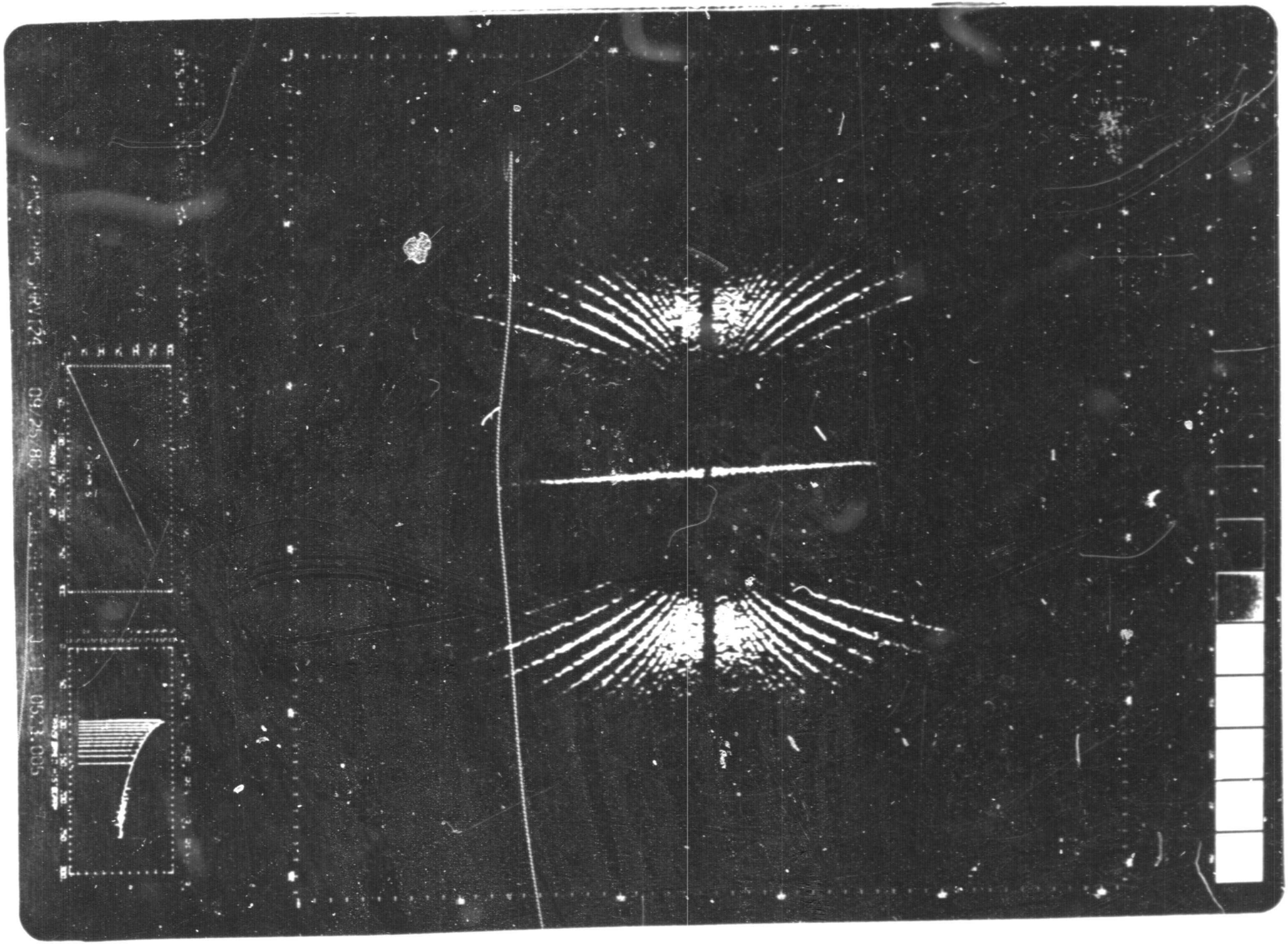

Fig. 9

26 May 1980

↓ with fore shortening corr. ↓ no foreshortening correction

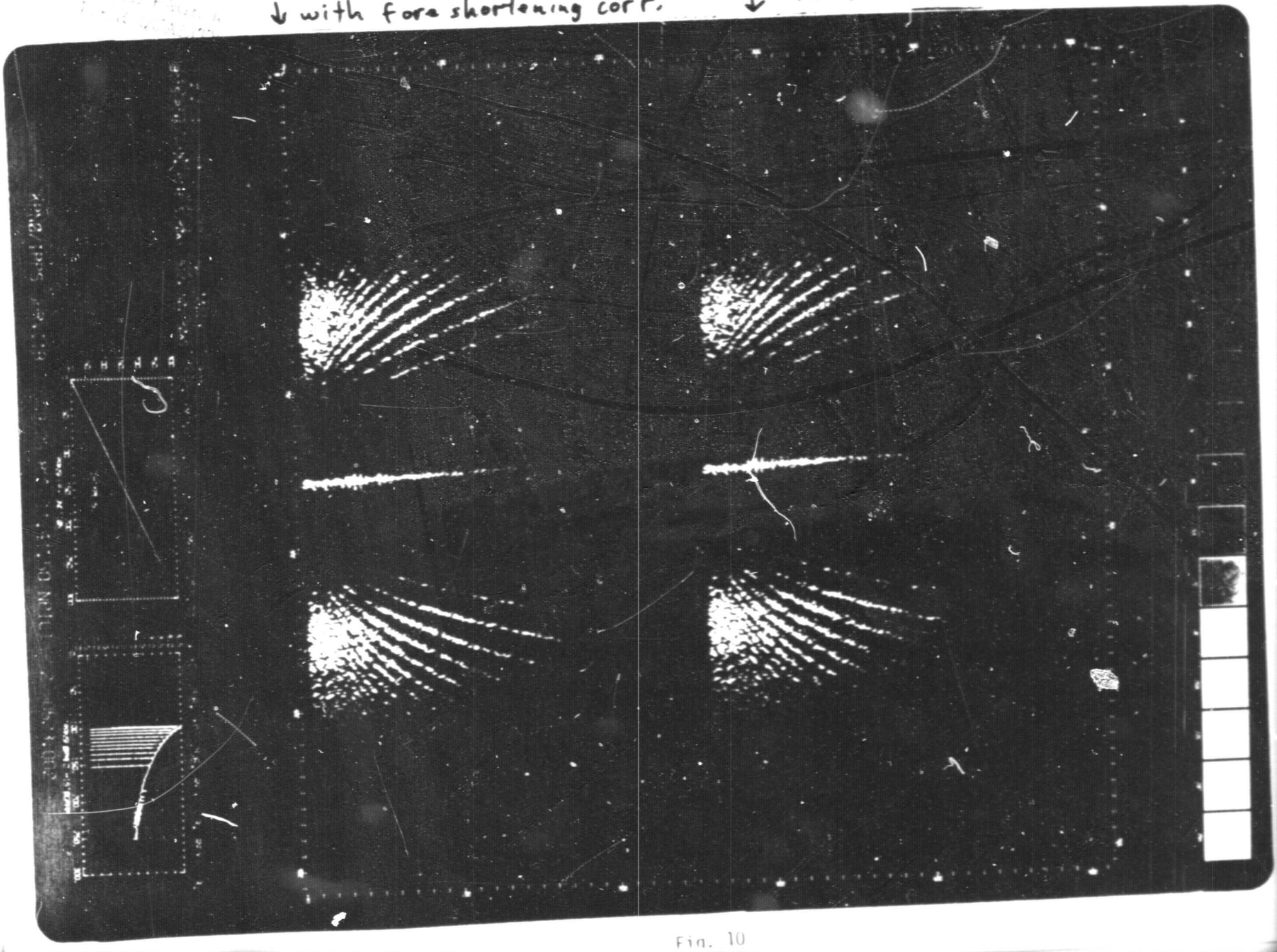

Fig. 10

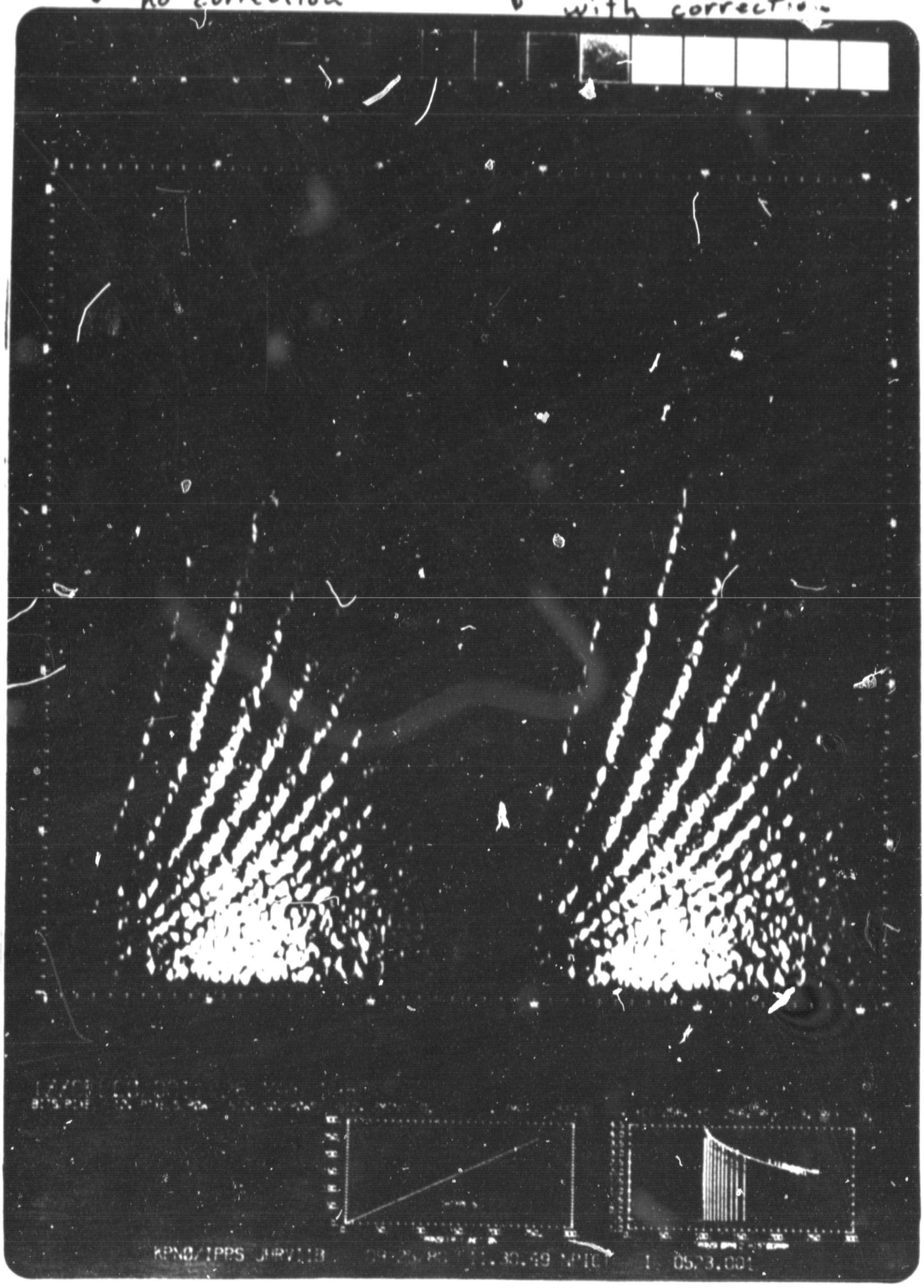
↓ no correction
↓ with correction

and decay properties of the p-modes. In addition to combining the spectra from successive days into one averaged spectrum, we have also directly compared the two separate power spectra in a search for systematic changes in the distribution of power along the p-mode ridges. Figure 12 shows the central portions of the May 26 and May 27 spectra. The two spectra are somewhat different; however, there are no obvious systematic shifts in power along the ridges from May 26 to May 27. This is shown in a different way in Figure 13 where the difference between the two power spectra is shown plotted in a gray level display. While there is some suggestion of modes that are strong on one day and weak on the next, there does not appear to be any overall pattern to the differences. On the other hand, there does appear to be some difference in the appearance of the difference map between the top and bottom halves of the spectrum, with small-scale features being slightly more pronounced and regular in the lower half of the difference map. Clearly, more detailed analysis of these two days' data strings, along with the analysis of the data from the three following days, will be needed before any conclusions on temporal variability can be made. In particular, the possibility that the power differences are simply due to the beating of unresolved modes within each resolution element must be examined carefully.

In addition to studying the properties of the mode themselves and of the solar interior, observations of p-modes can be useful in probing the structure of the solar chromosphere. Figure 14 shows that p-mode oscillations were first identified as such in the chromosphere through simultaneous observations in the photosphere (λ5576) and at an elevation of about 1000 km (from Rhodes, Ulrich, and Simon, 1977b). The right-hand spectrum in this figure is a p-mode spectrum obtained from velocity observations in the photosphere at λ5576, while the left-hand spectrum was obtained from measurements of the central intensity of λ8542. The same theoretical eigenfrequencies have been plotted through both spectra to illustrate that the same eigenfunctions are responsible for the oscillations at both elevations. The power does appear, however, to be shifted along the ridges to higher frequencies in the chromospheric spectrum relative to the photospheric spectrum.

The data shown in Figure 14 were obtained in 1975 at Sacramento Peak. The most recent data on the presence of the p-mode oscillations at chromospheric elevations is contained in Figure 15. This figure is a velocity power spectrum obtained with the CID camera at Kitt Peak in λ8542. The p-mode ridges are much more sharply defined here and suggest that we should eventually be able to study the relative velocity amplitudes of the different p-modes at the different elevations. In this way the predictions of the theoretical eigenfunction calculations can be directly compared with the observations. Later

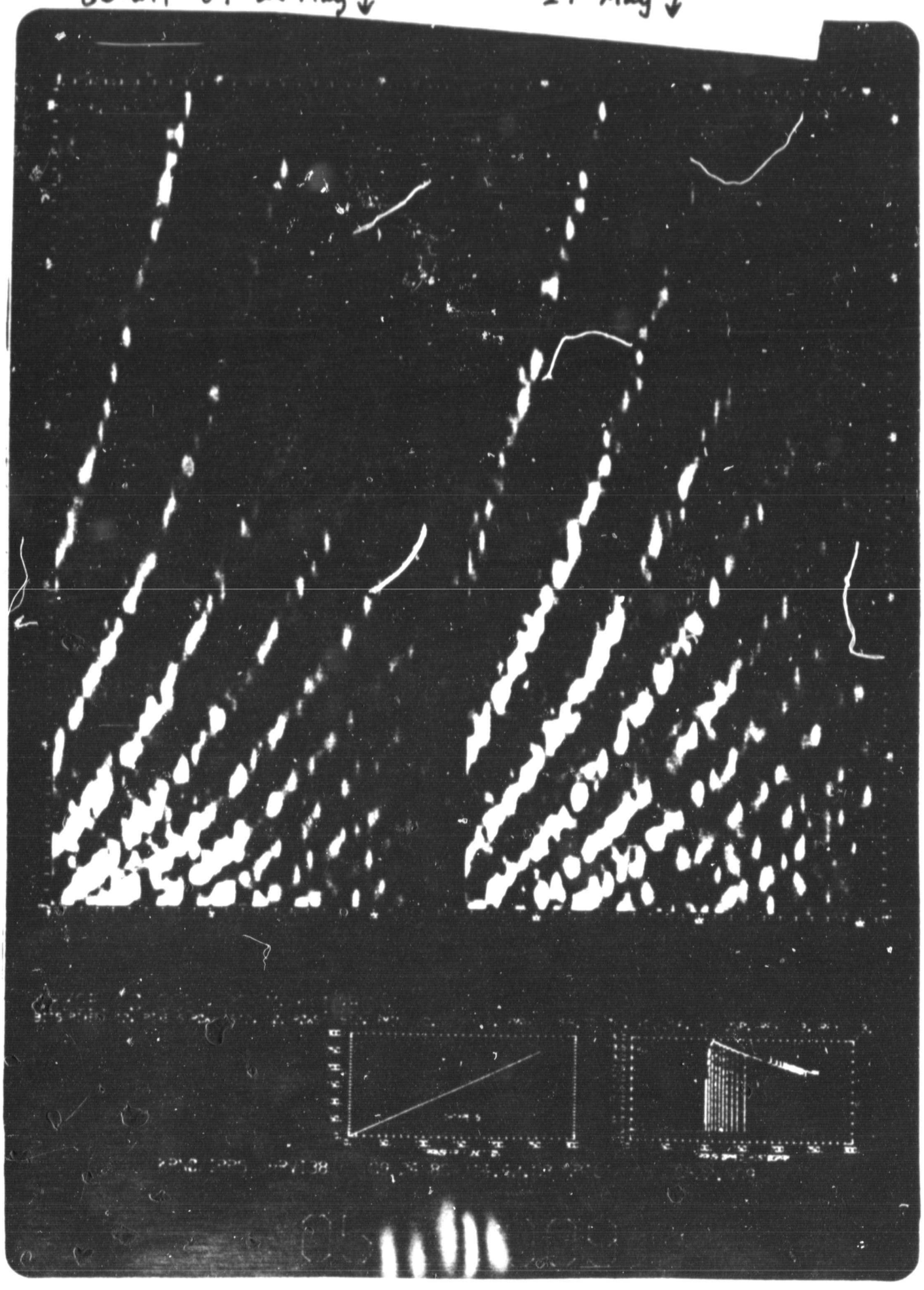

Fig. 12

26 May – 27 May 1980

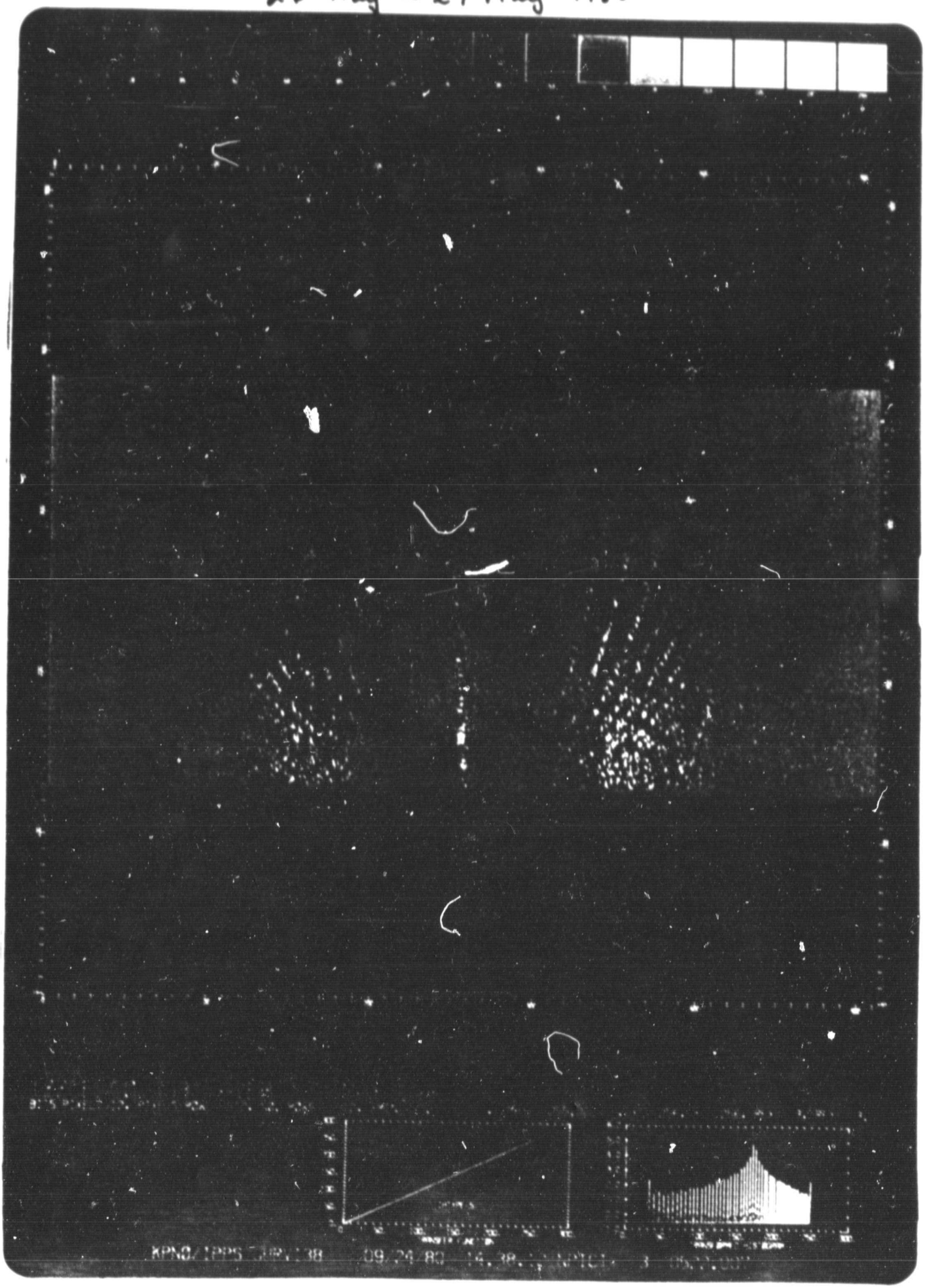

Fig. 13

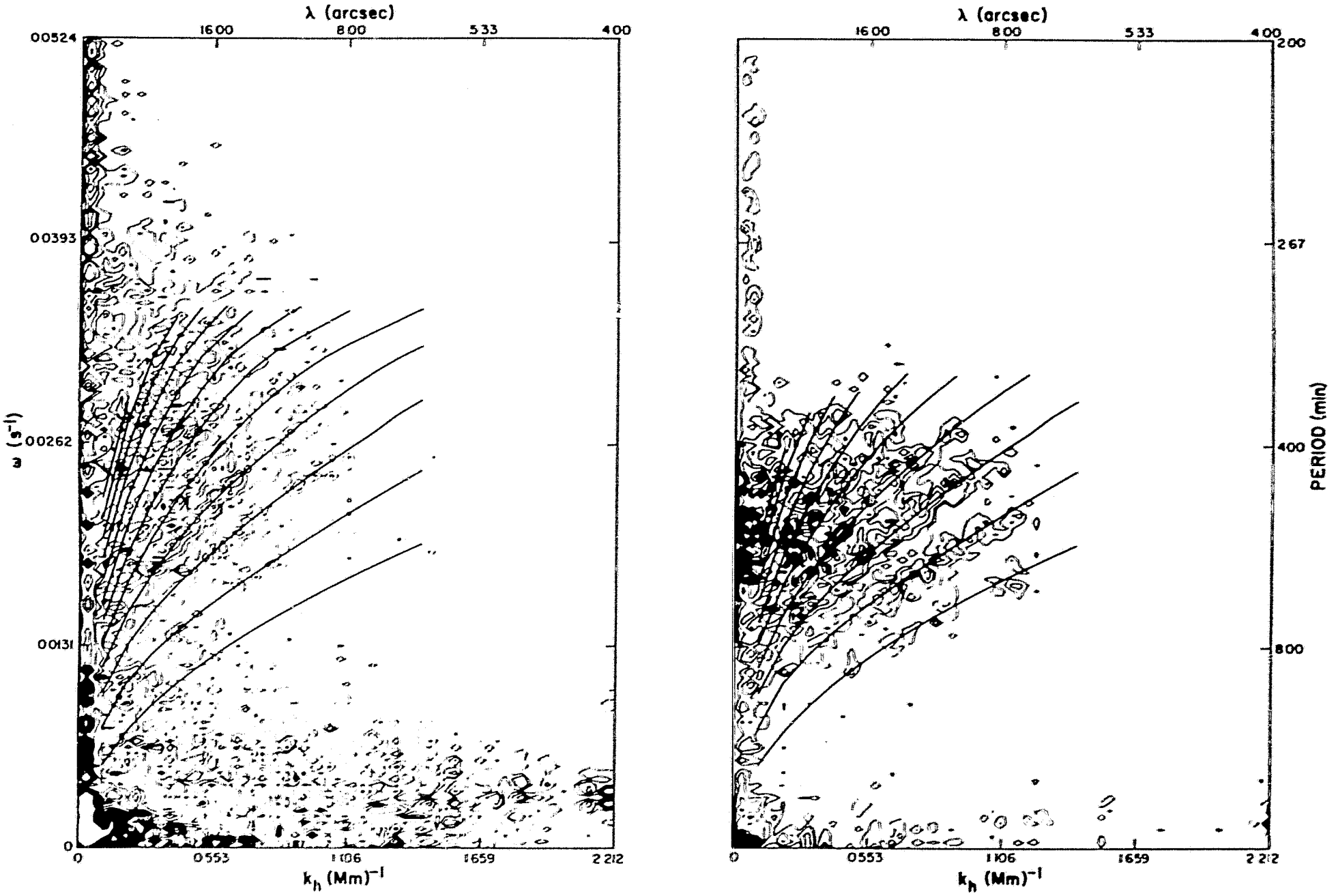
λ (arcsec)
1600
800
533
400
00524
00393
00262
00131
0
ω (s⁻¹)
0
0553
1106
1659
2212
k_h (Mm)⁻¹
λ (arcsec)
1600
800
533
400
200
267
400
800
PERIOD (min)
0
0553
1106
1659
2212
k_h (Mm)⁻¹

Fig. 14

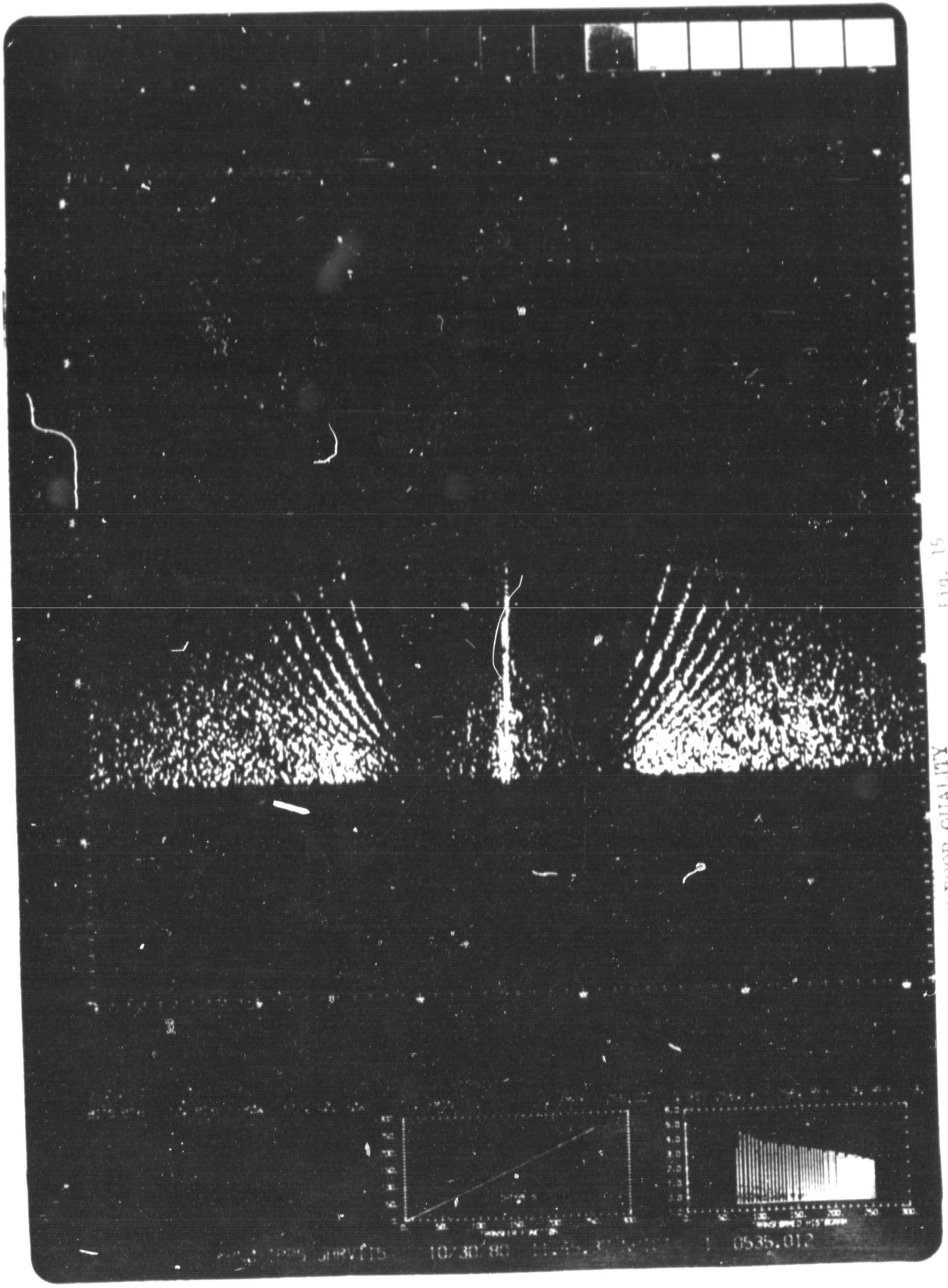

Fig. 15

Kitt Peak observations may allow such height-dependence studies to be made using different places in the wings of λ8542 or alternatively the equipment may allow simultaneous measurements of the velocity to be made in two different spectral lines.

The latest Kitt Peak observations are in excellent agreement with theoretical frequencies computed from envelope models having $1.7 \leq \ell/H \leq 2.0$ as is shown in Figure 16. The contours are the October 22 and 24 1979 averaged power spectrum, while the upper set of ridges came from the $\ell/H = 1.7$ model and the lower set were from the $\ell/H = 2.0$ model. We are now studying the effects of the distortion and foreshortening corrections before we attempt to select a "best-fitting" model.

2.2 Low-Wavenumber Modes

The first observations of radial ($\ell=0$) and near-radial ($1 \leq \ell \leq 4$) p-modes in the 5-minute portion of the spectrum were those of a University of Birmingham team (Claverie, et al., 1979). Using a potassium resonance cell instrument, with which they were able to make high-sensitivity Doppler observations of the sun seen as a star, Claverie and colleagues were able to obtain the one-dimensional power spectrum shown as Figure 17. This power spectrum was computed through the combination of observations made on two successive days into a single time series of 32 hours in duration within which zeroes were entered whenever data was not actually available. Claverie and coworkers identified the strongest spikes seen in this spectrum as p-mode waves having between 17 and 29 radial velocity nodes in the solar interior and having ℓ values equal to zero and one. The strongest spike in this spectrum is nearly centered on the frequency corresponding to a period of five minutes ($f = 3.3$ mHz), while other spike amplitudes decrease rapidly toward both higher and lower frequencies. However, since some of the structure seen in Figure 17 is due to the observing window available during the summer from Izana, Tenerife, where the observations were obtained, it would clearly be desirable to obtain continuous, uninterrupted observing runs extending at least over 32 hours and preferably longer.

Earlier this year the first such observations were obtained by a joint U.S.-French expedition to the South Pole which extended from November through February, 1979, 1980, (Grec, Fossat, and Pomerantz, 1980a). This team used a sodium resonance cell to obtain full-disk, integrated light velocity measurements of the sun for continuous runs of up to five days in duration. The power spectrum which resulted from analyzing a three- and- one-half-day-long segment of the 120-hour run is shown as Figure 18. This spectrum clearly confirms the existence of the oscillation modes claimed previously by Claverie, et al. (1979); in addition it demonstrates the dramatic improvement in spectral resolution available from an 82-hour, uninterrupted observing run in comparison with 32-hour, interrupted run. As in Figure 17, the observed power is highest near a frequency of 3.3 mHz

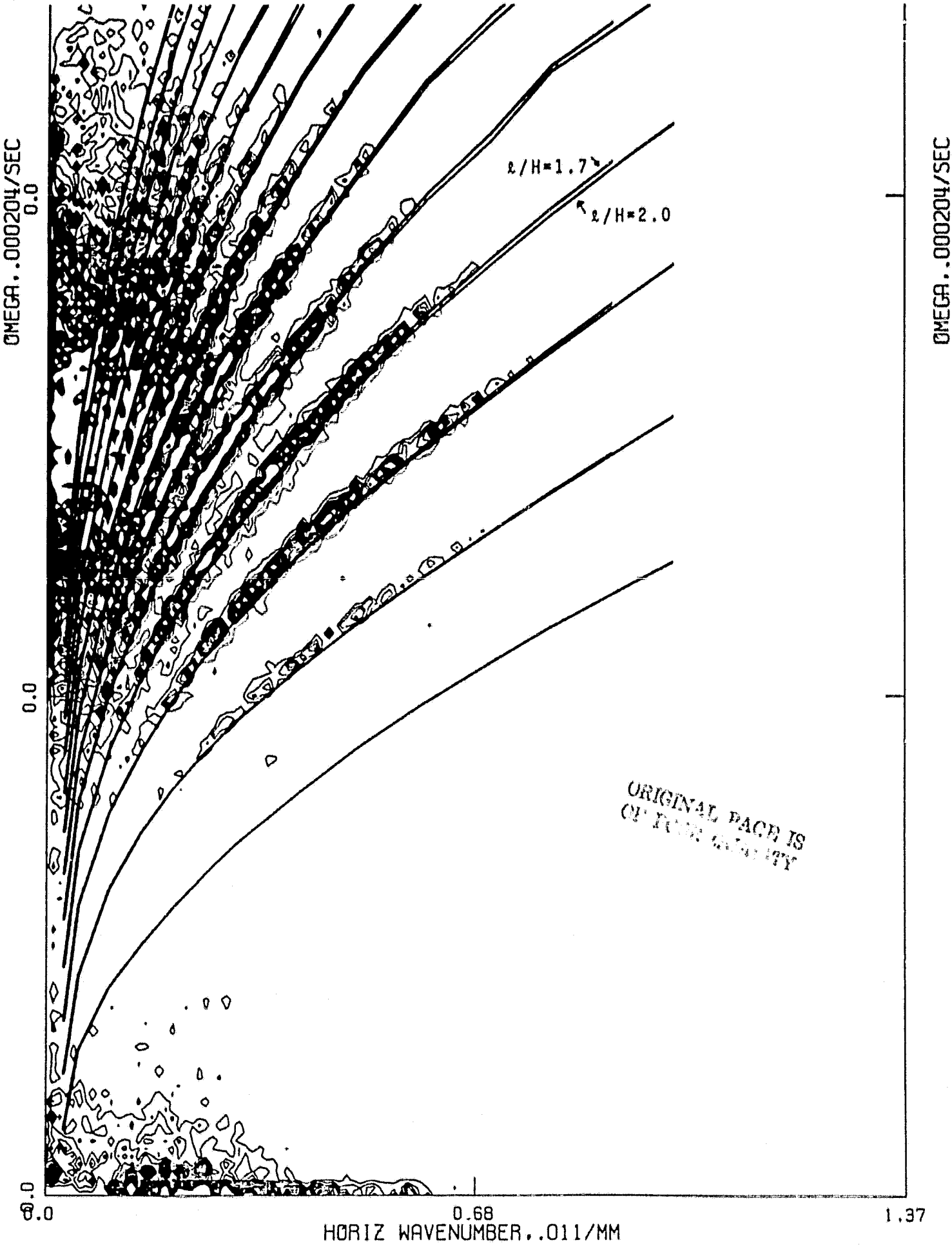

Fig. 10

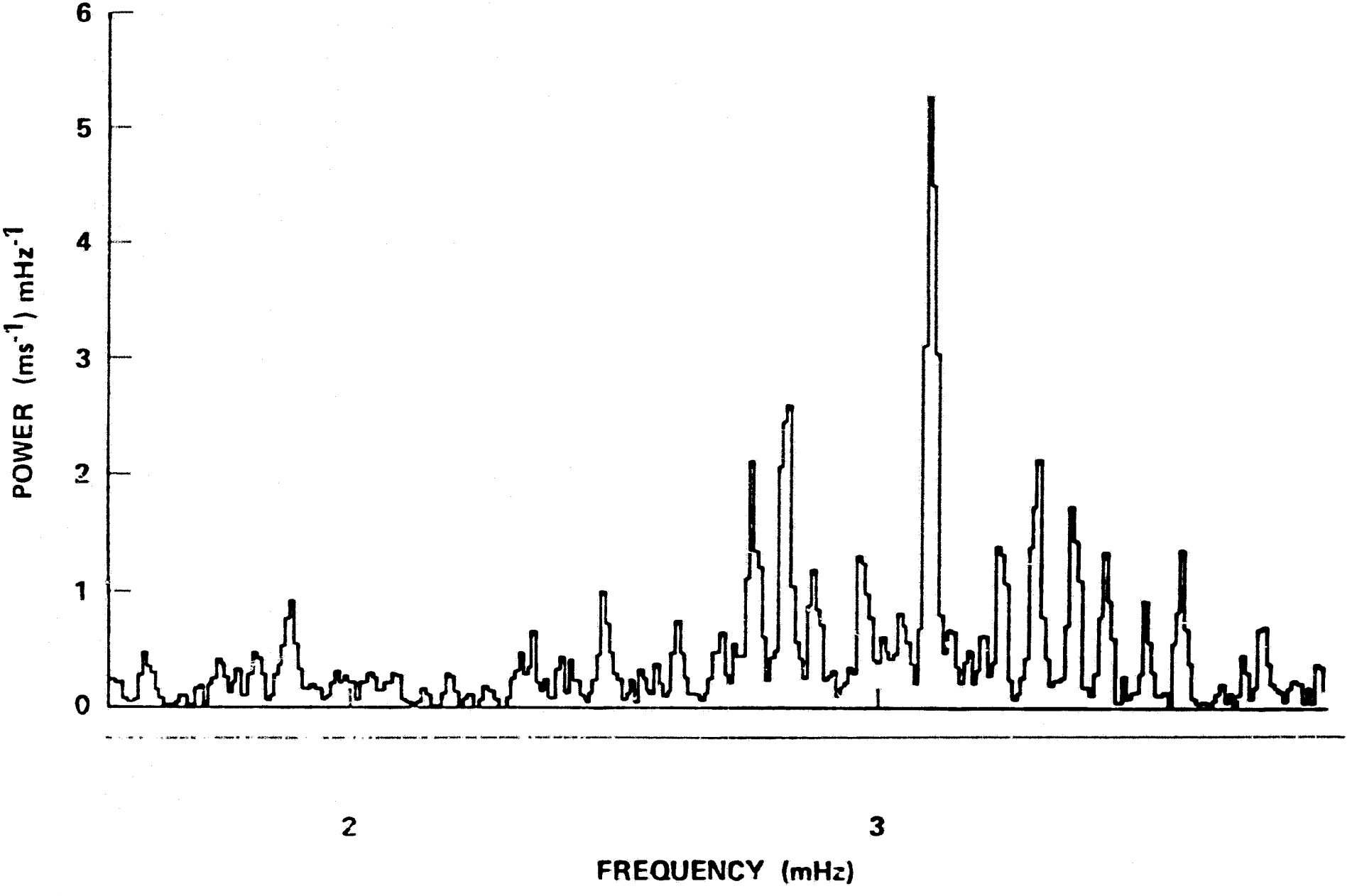

Fig. 17

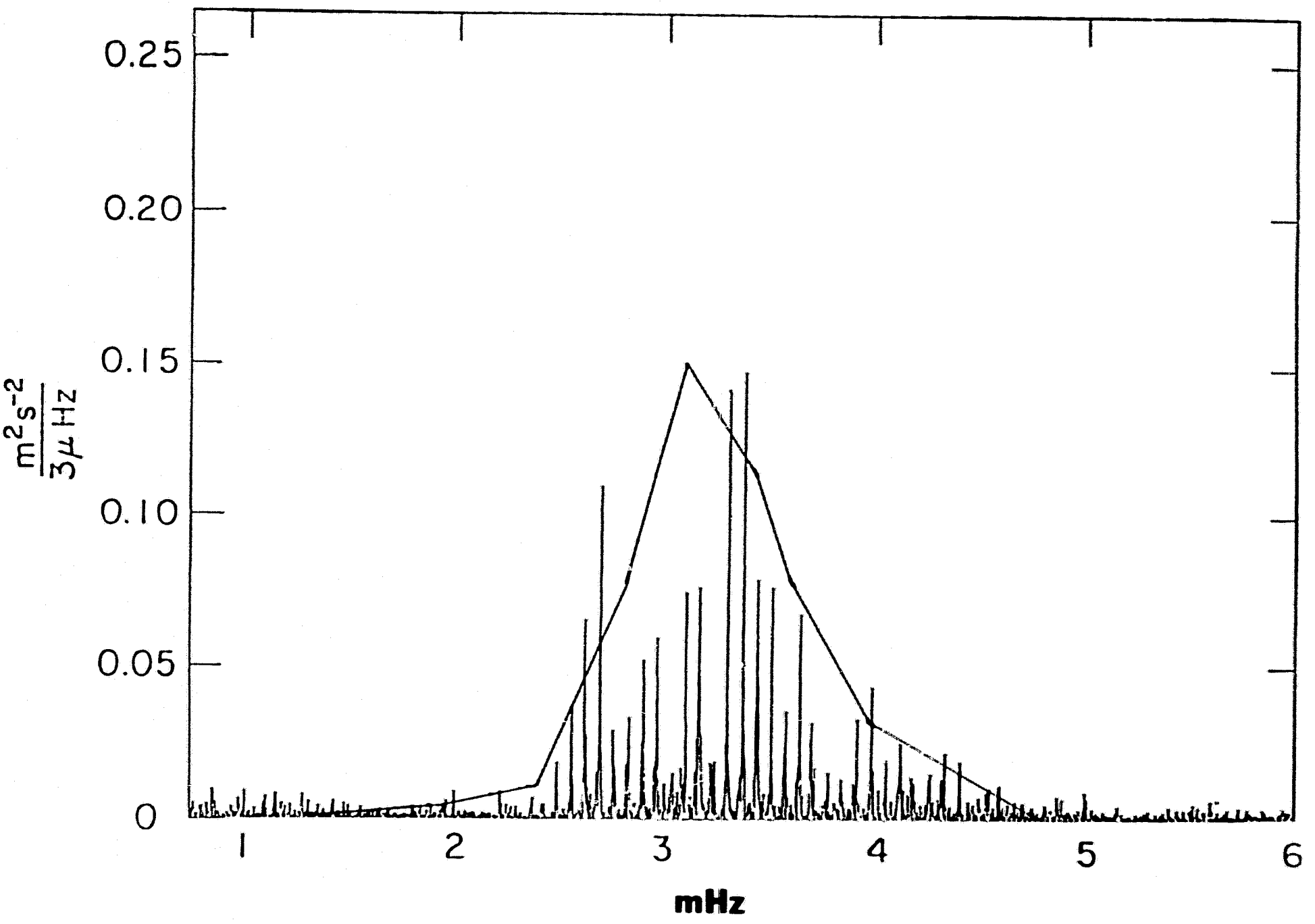

Fig. 18

and falls off toward higher and lower frequencies. The solid curve superimposed upon the observed power spectrum is the (normalized) relative power distribution obtained for the high-wavenumber p-modes by Rhodes, Ulrich, and Simon, (1977a). This comparison suggests that the relative observed amplitudes of both low- and high-wavenumber p-modes are determined by a common limiting mechanism.

3. Current Theoretical Status

3.1 Extended Envelope Models

The availability of the new South Polar data has provided a new and different set of observational criteria against which all current and future solar models must be tested. Furthermore, the existence of radial and low-degree non-radial p-mode oscillations means that extreme care must be exercised in the computation of the models which are used to calculate their structure and frequencies. Specifically, the radial and near-radial p-mode waves displayed in Figures 17 and 18 are permitted waves over almost the entire interior of the sun, in contrast to the higher-ℓ p-modes, which are only permitted near the solar surface. Consequently, computation of the theoretical eigenstructure of such deeply-penetrating oscillations requires the computation of complete, or nearly complete, solar models (i.e. models which extend over all or almost all of the suns radius), in contrast to the less complete models required for the higher-ℓ modes.

As illustrated previously in Figure 3, solar envelope models do not generally extend inward to the solar center. On the other hand, complete solar models calculated with a traditional stellar interior code do extend over the entire radius of the sun. However, as illustrated in Figure 19, such bi-directional integration codes usually do not treat the radiative transfer properties of the outer solar atmosphere insufficient detail for the computation of non-adiabatic oscillations. While the simplifications made in the atmosphere do not make large errors in the structure of the interior portions of the models themselves, they can result in the incorrect calculation of p-mode eigenfrequencies.

Because of this inconsistency, we chose to modify the model envelope code so that it could calculate closer to the center of the sun that it previously did. The properties of the models which resulted from this version of the program are illustrated schematically in Figure 20. The inward integrations were stopped approximately two percent of the radius away from the center; however, the outer atmospheric structure could now be used for deeper-penetrating p-modes than could the earlier envelope models. The solar radius was matched in these models; however, the solar luminosity was not yet calculated self-consistently.

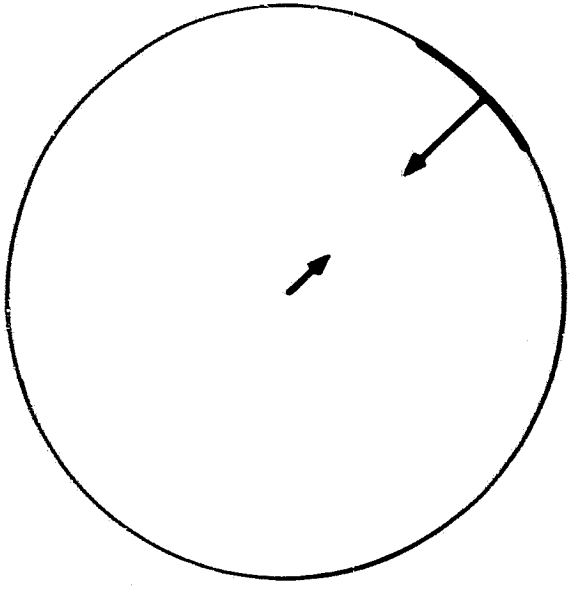

TRADITIONAL INTERIOR
(EVOLUTIONARY) MODEL

- $\ell/H \approx 1.7$, $x = 0.73$, $z = 0.02$
- INWARD AND OUTWARD INTEGRATION SOLUTIONS MATCHED AT SAME RADIUS
- BASE OF CONVECTION ZONE $\approx 0.73\ R_\odot$
- BUT OUTER ATMOSPHERE NOT TREATED IN ENOUGH DETAIL FOR OSCILLATION CALCULATIONS

Fig. 19

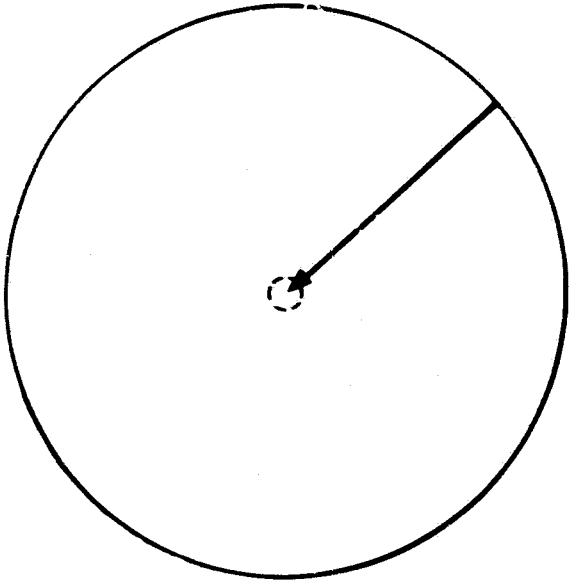

EXTENDED ENVELOPE MODELS

- INTEGRATIONS EXTENDED TO WITHIN 2% OF CENTER OF SUN
- ONLY MODEL WITH $\ell/H \approx 1.7$ IS NOW CONSISTENT WITH AMOUNT OF MASS REMAINING AT CENTER, CONVECTION ZONE BASE $\approx 0.73\ R_\odot$
- BUT LUMINOSITY NOT CALCULATED AT ALL

Fig. 20

Comparisons of the inner temperature profiles calculated from several of these extended envelope models with the temperature profile of the "standard" solar model which resulted from the solar interior (evolutionary) program are contained in Figure 21. The "standard" model curve is the solid curve. This model was obtained by using the current "best" values of nuclear reaction rates, opacity tables, and composition. The other three curves show the results of varying either the ℓ/H ratio of the model envelope or the interior opacity tables. The envelope model which most closely matches the interior temperature profile is that for $\ell/H=1.7$ with standard opacities ($k=1.0k_{st}$). This is the open-circle curve.

3.2 Comparisons with Observed Power Spectra

The adiabatic p-mode eigenfrequencies which were computed with the $\ell/H=1.7$, standard opacity model of Figure 21 for $0 \leq \ell \leq 5$ are compared with the full-disk observations of Claverie, et al. (1979) in Figure 22. These frequencies were computed with the perturbation in the gravitational potential explicitly included in the equations and with an out-going wave boundary condition in the corona. The theoretical frequencies are designated by the vertical lines which pass through the observed spectrum. The frequencies of the six different ℓ-values give the appearance of two separate multiplet patterns (one with two lines for the $\ell=1$ and 3 modes and another with four lines corresponding to $\ell=0$, 2, 4, and 5). Specific model identifications are given on an expanded scale for the 2.8-3.0 mHz frequency interval in the legend at the top of the figure. In this legend the lines for the different ℓ-values are drawn with different lengths to aid in matching the ℓ-values with their frequencies. However, the linear pulsation code used to generate the frequencies does not predict the relative amplitudes of the different modes. Consequently, the lengths of the theoretical lines drawn through the observational spectrum are entirely arbitrary. The overall agreement between the observations and the theoretical frequencies does support the identification of successive spikes as alternately odd or even ℓ-value modes; however, the frequencies shown were calculated with a "standard" envelope model as described above rather than with a low-z model as suggested by Claverie, et al. On the basis of this comparison, we previously concluded that a standard model does an adequate, though not perfect, job of fitting these observations (Rhodes and Ulrich, 1980). Different envelope models corresponding to ℓ/H values different than 1.7 to 2.0 would have their predicted eigenfrequencies located between the observed peaks rather than nearly coincident with them as shown here.

Clearly, higher observational frequency resolution would allow us to tighten this comparison between observation and theory. Hence, we have also compared the theoretical frequencies of Figure 22 with the South Polar data of Grec, Fossat, and Pomerantz. This comparison is shown in Figure 23. The theoretical frequencies for $\ell=0$ and 1

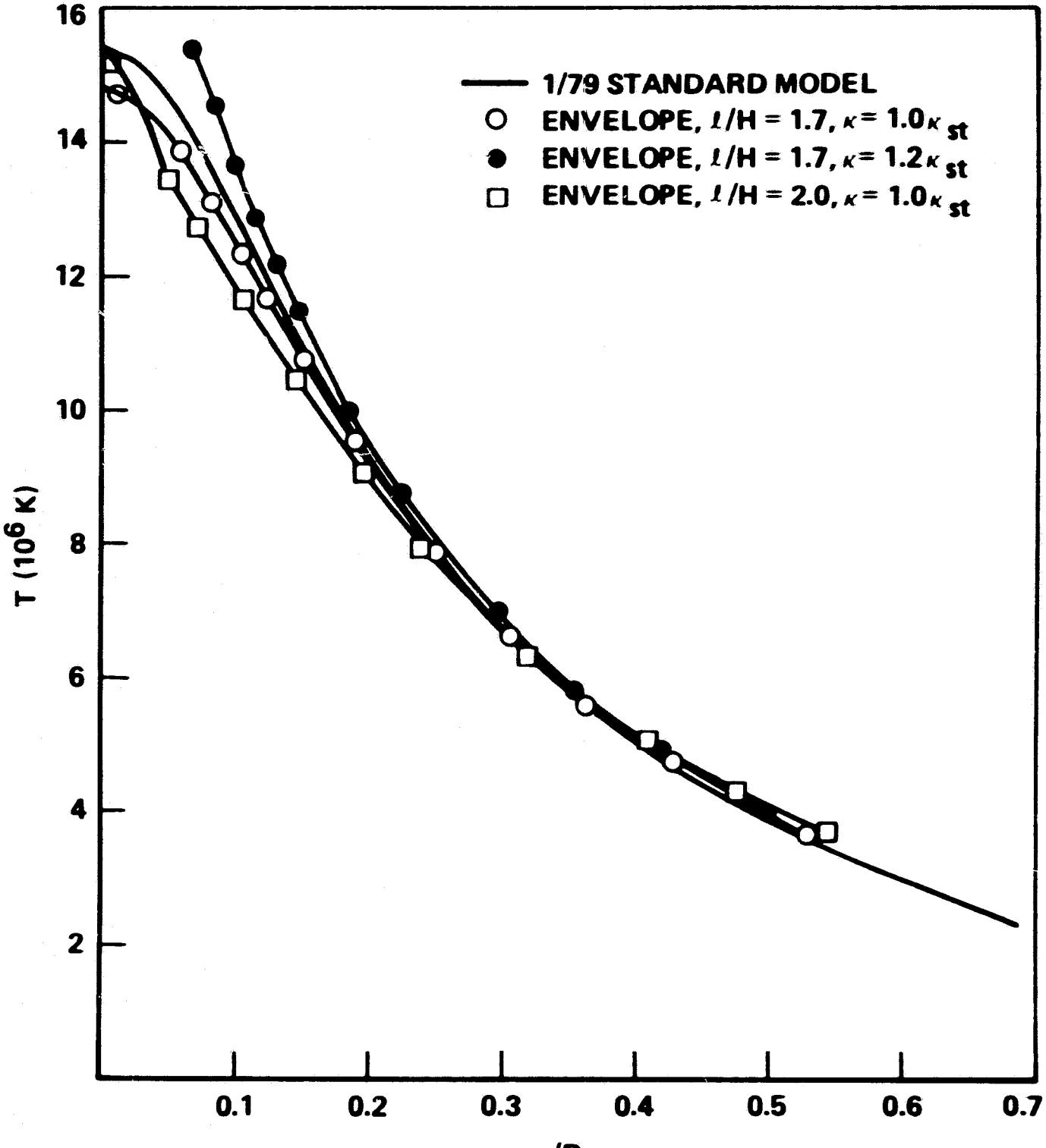
1/79 STANDARD MODEL
ENVELOPE, ℓ/H = 1.7, $\kappa = 1.0\kappa_{st}$
ENVELOPE, ℓ/H = 1.7, $\kappa = 1.2\kappa_{st}$
ENVELOPE, ℓ/H = 2.0, $\kappa = 1.0\kappa_{st}$
T (10^6 K)
16
14
12
10
8
6
4
2
0.1
0.2
0.3
0.4
0.5
0.6
0.7
r/Ro

Fig. 21

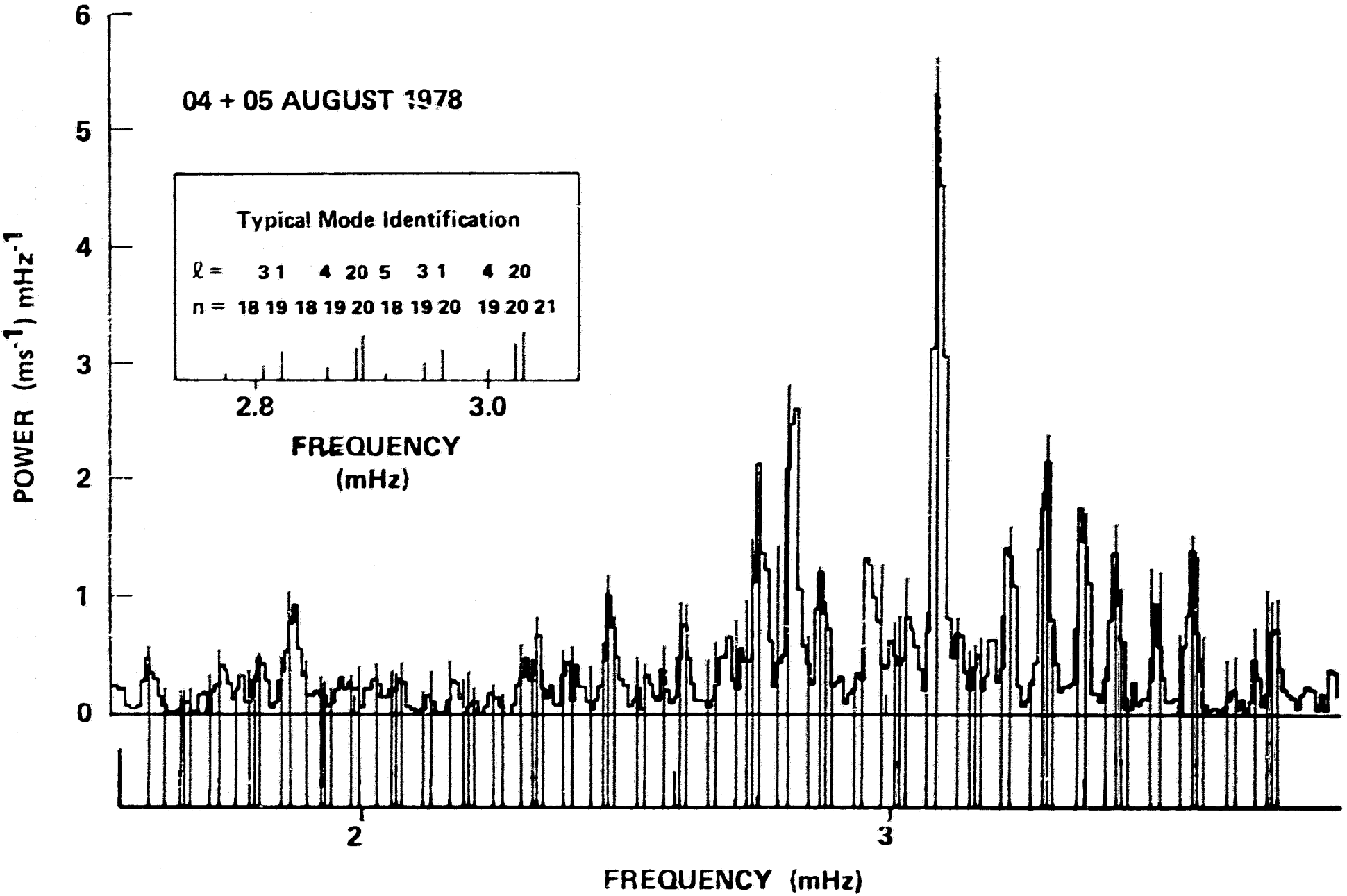
04 + 05 AUGUST 1978
Typical Mode Identification
ℓ = 3 1 4 20 5 3 1 4 20
n = 18 19 18 19 20 18 19 20 19 20 21
2.8
3.0
FREQUENCY
(mHz)
POWER (ms⁻¹) mHz⁻¹
6
5
4
3
2
1
0
2
3
FREQUENCY (mHz)

Fig.22

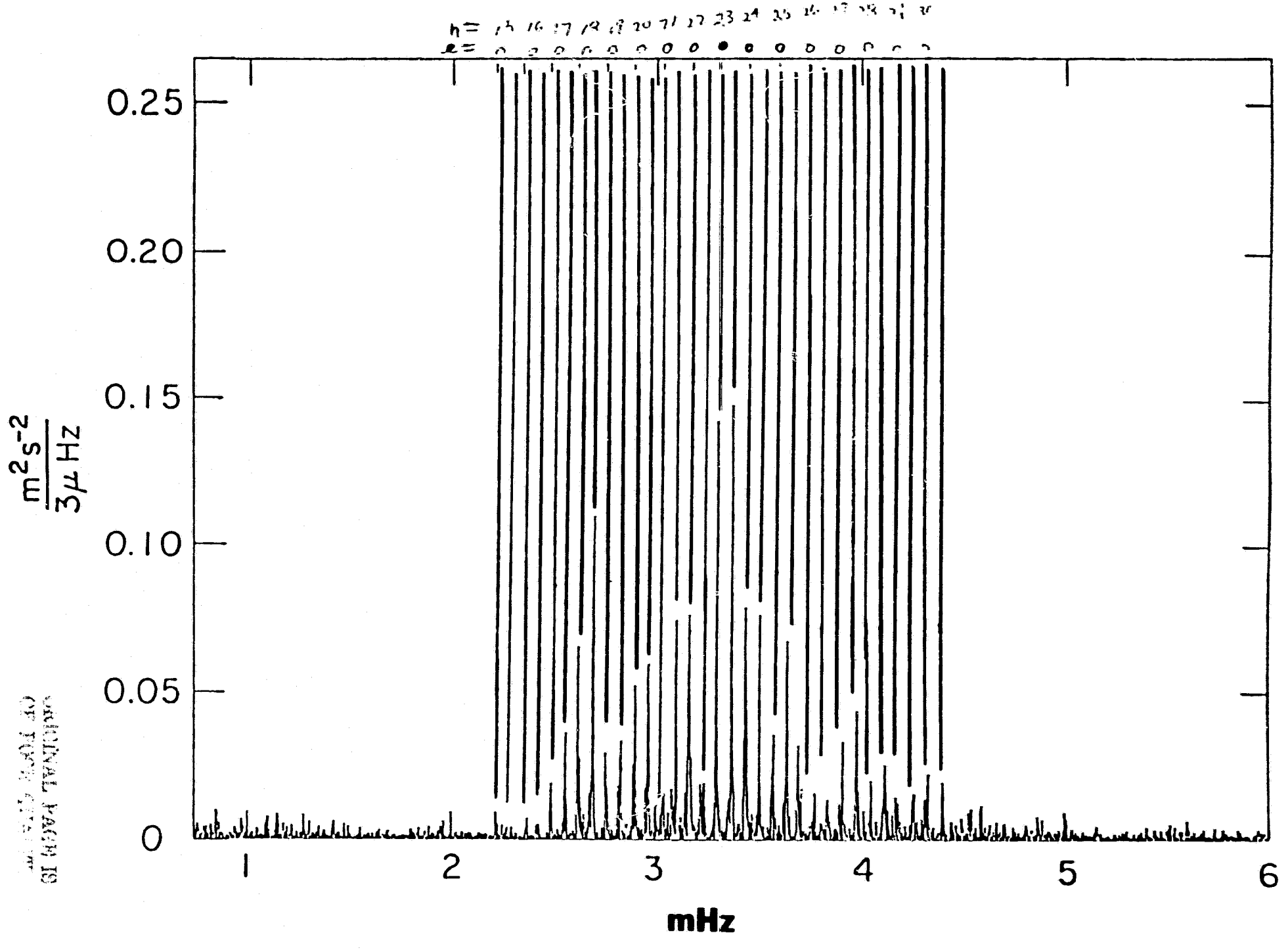

Fig. 23

are designated here as the long vertical lines running downward from the top of the figure to a point just above the observational spectrum at the bottom. (The modes for ℓ=2 and 3 would be nearly indistinguishable from the ℓ=0 and 1 lines on the scale of this figure.) The agreement between the observational spikes and the theoretical frequencies is definitely superior to that shown in Figure 22 and suggests that a standard solar model will ultimately fit all of the observational spikes. But the particular extended envelope model used to generate these frequencies must be modified slightly since the agreement between the observations and the theory worsens as the frequency increases above 2.5 mHz.

Before describing the remaining refinements which need to be made in the theoretical treatment of these modes, we show the comparison with the observational spectrum on an expanded scale in Figure 24. This figure shows the results of averaging the observational spectrum shown in Figure 23 in 136 μHz-wide segments (i.e., the spectrum shown is a superposed-frequency spectrum). The theoretical eigenfrequencies shown in the previous figures for n=19 are shown here as solid vertical lines marked ℓ=0 and ℓ=1, while the additional frequencies for ℓ=2, 3, and 4 are also shown as solid lines. The frequency separation between the ℓ=0 and ℓ=1 and ℓ=3 modes agrees very well with the average observational separation; however, the ℓ=0 to ℓ=2 and ℓ=0 to ℓ=4 separations are not as good. Much of the width of the observed peaks results from the fact that the actual frequency separations are not strictly constant over the range of n-values (15 to 30) which were included in the averaged spectrum.

Figures 23 and 24 show that additional refinements in the theoretical treatment of the oscillations will be necessary before the comparison between theory and observation will match the accuracy of the best available observations.

3.3 Complete Solar Models

In a further attempt to improve the agreement between the observed and theoretical frequencies, we next modified our envelope model code to make it more consistent with the stellar interior code. As illustrated schematically in Figure 25, these changes included provision for the explicit calculation of the energy generation due to the nuclear reactions in the solar core. A second change was the introduction of an iterative method by which initial values of the ℓ/H ratio and hydrogen mass fraction, x, could be simultaneously iterated upon in order to match both the solar radius and luminosity. After incorporating these changes, we were no longer free to choose values of ℓ/H or x arbitrarily as we could when the solar luminosity was not explicitly calculated.

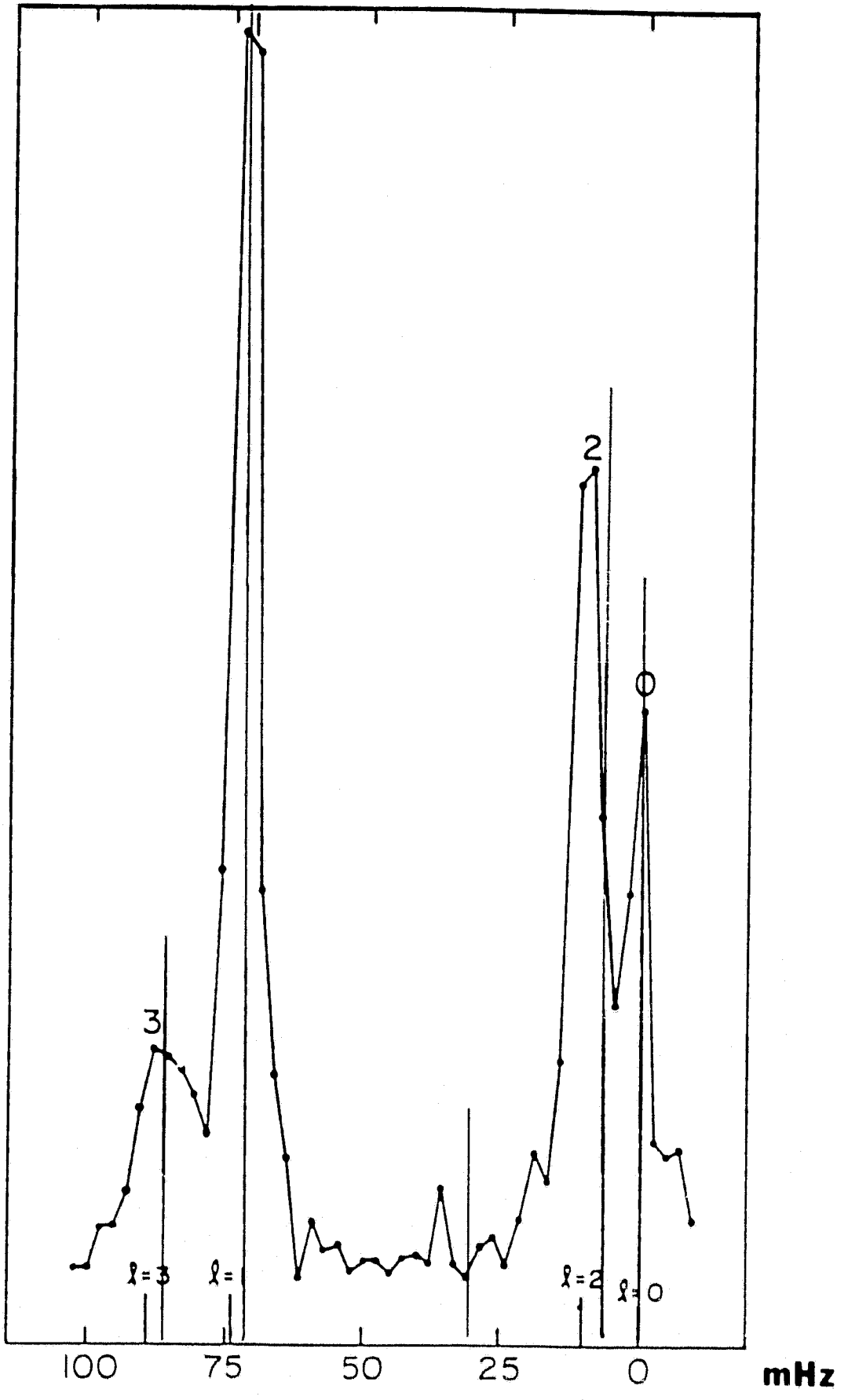

Fig. 24

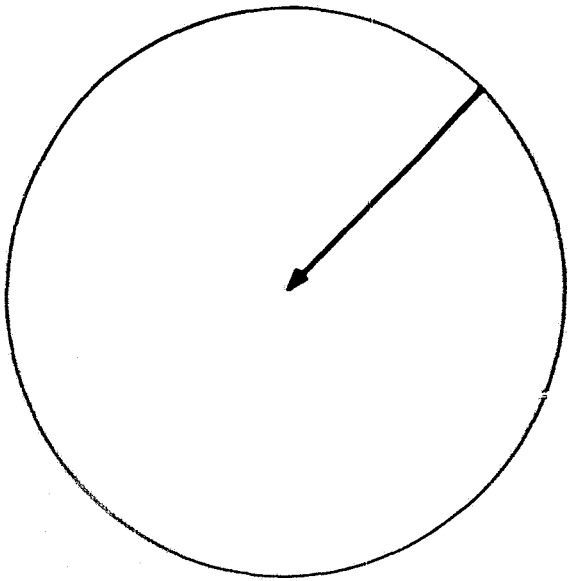

- SELF-CONSISTENT COMPLETE SOLAR MODELS FROM ENVELOPE CODE.
- NUCLEAR ENERGY GENERATION NOW CALCULATED EXPLICITLY AS IN EVOLUTIONARY MODELS
- INWARD INTEGRATION COMPLETELY TO CENTER
- MODEL ITERATED TO CORRECTLY MATCH $R_\odot$ AND $L_\odot$

$\ell/H = 1.91$, $T_c = 15.4$, SNU = 9.5

$x = 0.7302$, $z = 0.018$

Fig. 25

The properties of the "standard" solar model which resulted from inputting the opacity tables of W. Heubner and his colleagues at Los Alamos, the latest nuclear reaction cross sections, and a metal abundance, z, of 0.018 are shown in Figure 25. They include an ℓ/H ratio of 1.91, a central temperature of 15.4 million degrees, a solar neutrino rate of 9.5 SNU, and hydrogen mass fraction, x, of 0.7302. The convection zone depth of this model was 27.1 percent of the solar radius.

We wish to note here that the specific value of ℓ/H which results from this iterative procedure depends critically upon the outer atmospheric structure, while the depth of the convection zone is not sensitive to the outer atmospheric structure. Specifically, when the chromosphere and corona were removed from the model, the ℓ/H value which resulted was decreased from 1.91 to 1.32, while the convection zone depth was unchanged. Thus, the specific value of ℓ/H given above is probably not important, while the depth of the convection zone is significant.

Once the envelope code had been made self-consistent in this fashion, we could then use it to compute various "non-standard" solar models. In particular, we chose to compute a so-called "dirty" solar model, (see Christensen-Dalsgaard, Gough, and Morgan, 1979, for a general discussion of such models). In this model we left the metal abundance in the convection zone equal to the observed value of 0.018, with the distribution of elements as given by Ross and Aller (1976). However, interior to the base of the convection zone we reduced the metal mass fraction to 0.3 times the surface value. We then matched the current solar radius and luminosity with the iterative procedure described above. The properties of the intermediate - z model which resulted are tabulated in Figure 26. The ℓ/H value was decreased slightly to 1.74, while the hydrogen mass fraction, x, was increased to 0.82.

Somewhat surprisingly we found that the structural differences between the non-standard and standard models were principally limited to the radiative interior below the convection zone. Above the base of the convection zone, where the two models had the same composition, the structures of the models were almost identical as illustrated schematically in Figure 26. In fact, the convection zone depth was essentially unchanged in the two models. Below the convection zone, however, the non-standard model had a lower temperature at every radius than did the standard model as illustrated in Figure 26. The central temperature of the "dirty" model was decreased from 15.4 to 13.8 million degrees. Correspondingly, the SNU rate was reduced down to 1.6.

The fact that the two models had nearly identical convection zone structures meant that the high wavenumber p-mode eigenfrequencies (i.e. for $k_h \geq 0.2$) calculated from each model were also almost

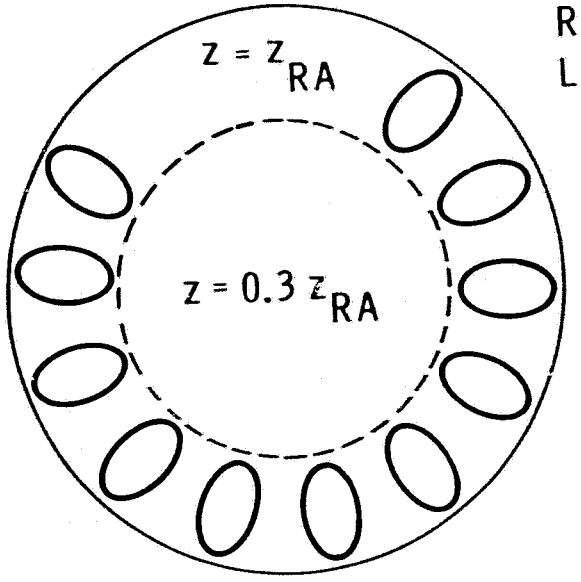

$R = R_\odot$
$L = L_\odot$

INTERMEDIATE-z
"DIRTY" SOLAR MODEL

$\ell/H = 1.74$
$T_c = 13.8$
SNU = 1.6
x = 0.82

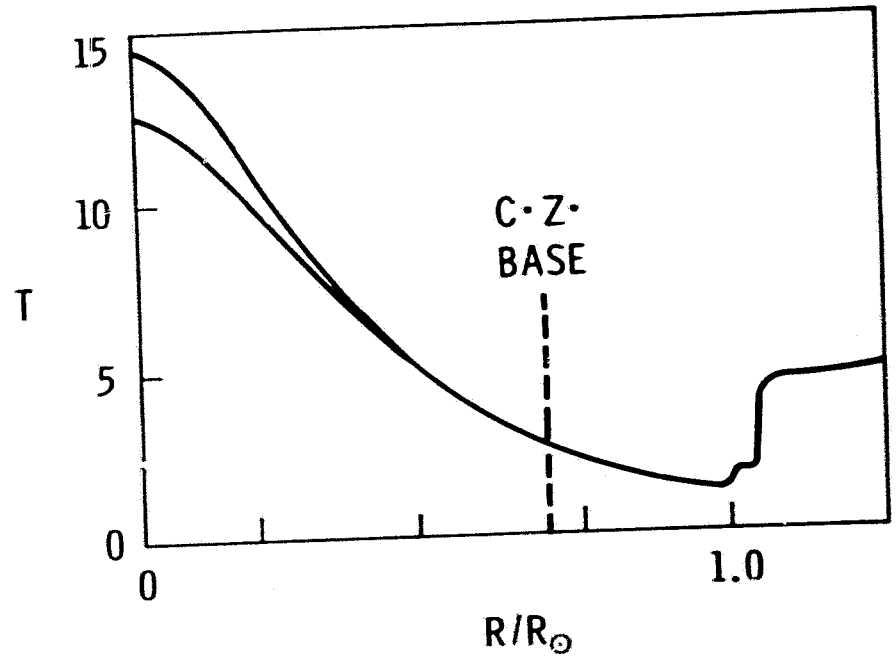

ESSENTIALLY IDENTICAL
CONVECTION ZONE STRUCTURE
IN "STANDARD" AND INTERMEDIATE
z MODELS

BASE AT $\approx 0.70\ R_\odot$

Fig. 26

identical. Thus, without an improvement in observational resolution of the p-mode ridges at such large wavenumbers, the only existing observations which could be used to discriminate between these two different models were the South Polar observations of Grec, Fossat, and Pomerantz. Accordingly, we computed eigenfrequencies for ℓ=0 and 1 for both the normal- and intermediate-z models. The frequencies of the non-standard model all fell below the standard model frequencies as illustrated in Figure 27 for 10 different ℓ=1 modes. Figure 27 repeats the Grec, Fossat and Pomerantz spectrum of Figure 23 and includes the theoretical eigenfrequencies for both of the models as the small marks above the observed spectrum. As is indicated in the legend, the longer marks correspond to the standard model while the shorter marks correspond to the non-standard model. Some of the observed spikes appear to fall between the two model frequencies, while others appear to agree better with the non-standard model; however, as we will now discuss, it is premature to use these theoretical frequencies to make any inferences about which model fits the observations better.

First of all, we have found that increasing the number of grid points in our models from roughly 200 to over 400 lowers the frequencies of these ℓ=0 and ℓ=1 modes for both models by such an amount that the standard model frequencies all fall slightly below the observed spikes, while the non-standard model frequencies fall even further below the observed spikes. Second, we have just begun to experiment with the non-adiabatic terms in the model analysis and have found that the conversion from an adiabatic to a non-adiabatic treatment of these high order radial and near-radial modes raises the frequencies just enough that the standard model eigenfrequencies are only 0.1 percent below the observed frequencies while the non-standard frequencies are still below the standard model frequencies. Clearly, more theoretical work remains to be done with the non-adiabatic treatment of the low-degree p-modes before any definite conclusions can be made as to which of these, or other possible non-standard models, best fits the observed power spectra at both large and small wavenumbers.

4. Needed Observational Improvements

4.1 Improved Resolution in k_h and ω

Improvements are needed in the observational resolution currently possible in the k_h-ω plane. At high wavenumbers the p-mode ridges need to be made narrower in ω than those shown in Figure 16 in order to more finely discriminate among the different models which give similar frequencies in this portion of the k_h-ω phase, where the frequencies are most sensitive to convection zone structure. Such improved resolution in ω can possibly be obtained by combining several days' of consecutive observations into one long data string with zeroes included during nighttime gaps; however, the sidelobes which

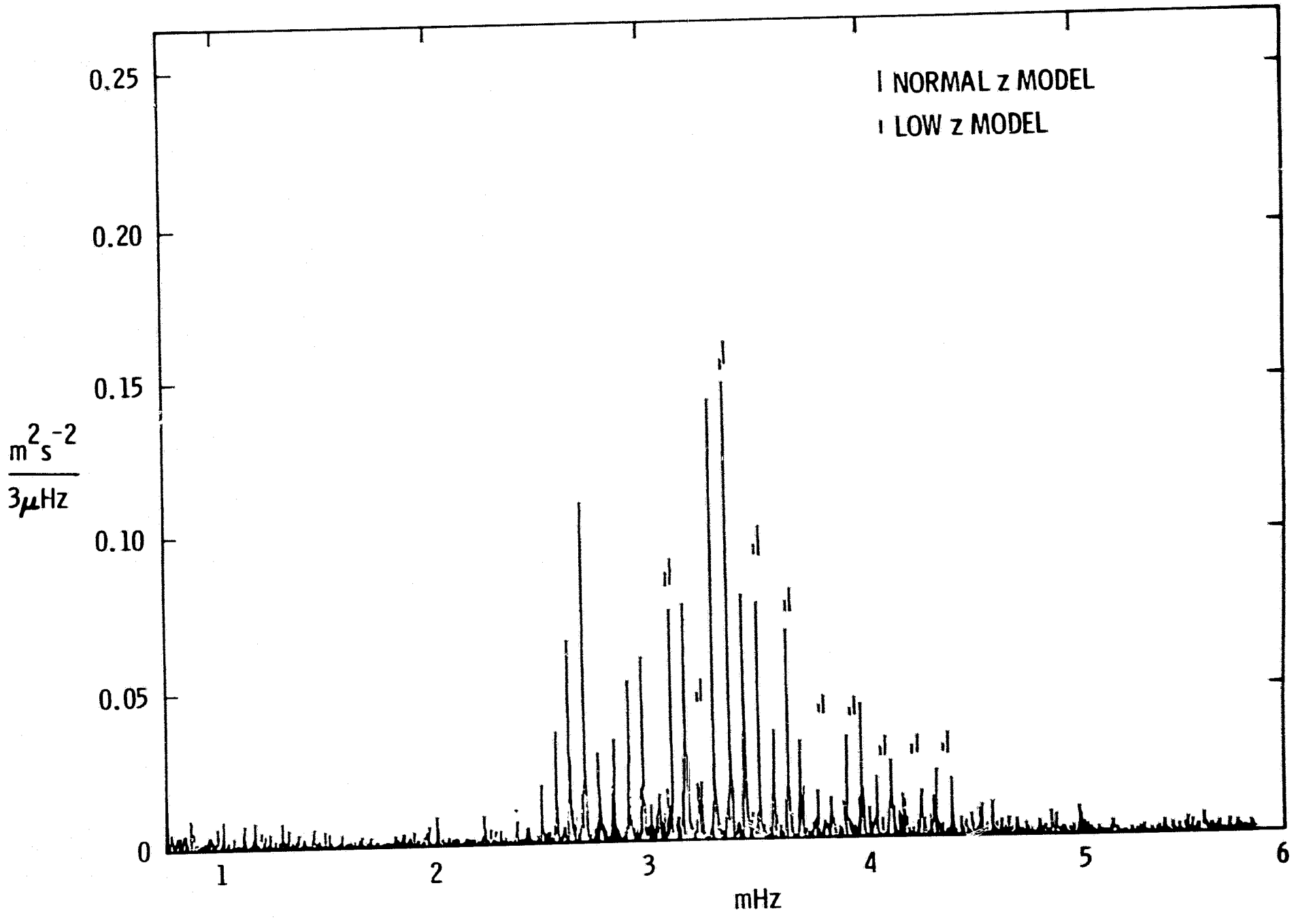
NORMAL z MODEL
LOW z MODEL
0.25
0.20
0.15
0.10
0.05
0
$m^2 s^{-2}$ / $3\mu Hz$
1
2
3
4
5
6
mHz

Fig. 27

will result from such an approach may offset the expected resolution gain. Careful experimentation will be necessary before this question can be answered. Alternatively, two-dimensional observations with a CID camera could be obtained for several uninterrupted days from the South Pole, but such a project would be a much more complicated undertaking than the simple resonance-cell observations obtained there to date. The third alternative would be to observe with a two-dimensional detector system from a sun-synchronous, polar-orbiting satellite.

At intermediate wavenumbers (corresponding to $5 \leq \ell \leq 150$) there is need for improved resolution in both ω and in horizontal wavenumber. Such increased resolution will be necessary to resolve the confusion between different modes which currently exists in this portion of the k_h-ω plane where the p-mode ridges are both strongly sloping and relatively closely-spaced. Resolution of the confusion in this area is crucial to any attempts at finding one solar model to fit all of the available frequencies from ℓ=0 to ℓ=1000. Before the remaining ambiguities between standard and non-standard models can be resolved, it will be necessary to test them in this intermediate-ℓ regime as well.

The comments made above regarding improved ω-resolution also apply here, while improvements in wavenumber resolution will require different solutions. The manner in which the available horizontal-wavenumber resolution depends upon the size of the region scanned on the sun is illustrated in Figure 28. This figure shows a cross-section of the sun as viewed from its north pole. The current east-west baseline available at Kitt Peak is illustrated as a total baseline of 0.66 $R_\odot$, which is shown to correspond to a total 9.5 separate ℓ values within each separate k_h-bin in a two-dimensional k_h-ω power spectrum. The confusion resulting from the inclusion of so many p-modes with each k_h-resolution bin was illustrated in the SCADM symposium held in Wellesley, Mass. (Rhodes, 1979). To improve the wavenumber resolution to the point that only three separate ℓ-values are isolated within each wavenumber bin, the figure shows that a baseline of 2 $R_\odot$ would be needed, which projects to 1.63 $R_\odot$ linearly across the solar disk. To obtain useful data over such an extended area, conversion from a rectangular to a spherical coordinate observing grid would be necessary to compensate for the severe foreshortening effects. Also, some allowance would have to be made for the non-radial components of the Doppler velocities and for the projection of these velocity vectors into the line of sight. All of these problems would entail massive amounts of computer manipulation of the data well beyond that currently being applied to such observations. An alternative approach would be simultaneous observations obtained from both the earth and from a spacecraft located 60 to 90° around the sun from the earth.

At the lowest wavenumbers available ($\ell \leq 5$) there is still a need for improved ω-resolution. We need to be able to separately resolve the ℓ=0 and 2 doublet and the ℓ=1 and 3 doublet without relying on

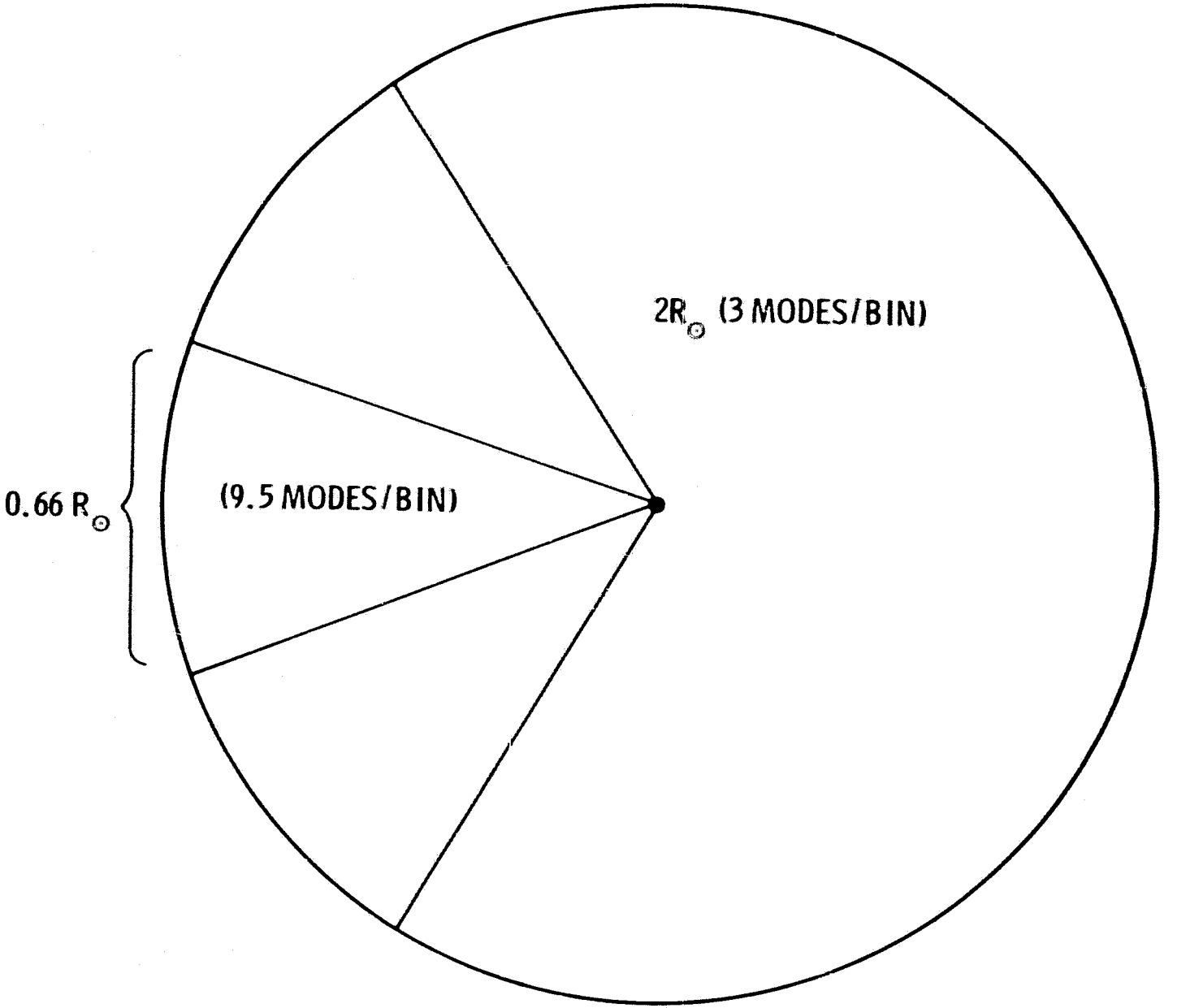

Fig. 28

frequency averaging before we will truly be able to say which set of theoretical frequencies best fits the observational frequencies.

4.2 Improvements in Rotational Velocity determination

Improvements in Rotational Velocity Determination as will be discussed in detail later in these proceedings (Rhodes, et al. 1980), the frequency splitting between eastward- and westward-propagating modes illustrated in Figure 9 can be used to measure the rate of solar rotation. Since the rotational velocity that is measured with this technique depends upon measurements of both the frequency splitting and of the horizontal wavenumber, improvements in our knowledge of both quantities will improve the accuracy of the velocity measurements. The frequency resolution can only be improved upon at the expense of longer-duration observing runs, which limit our ability to search for short-lived rotational changes. Also, improvements in wavenumber resolution will be difficult to obtain for the reasons just mentioned. On the other hand, to get the absolute wavenumber scale, we need to accurately know seemingly simple things such as the diameter of the solar image in the plane of the detector to better than 1% so that we can get the image scale in km per pixel to similar precision. We need to know where the limbs of the sun are relative to the detector for every frame of data to remove the effects of image motion and we need to measure the image distortion introduced by the optical system so that it can be removed along with the effects of foreshortening on the sun. Finally, since the deepest-going rotational velocity determinations are those made at the lowest-ℓ values, the resolution of the intermediate-wavenumber portion of the k_h-ω will also be necessary to obtain such measurements.

4.3 Chromospheric and Transition Zone Studies

More observations of the p-mode oscillations at chromospheric elevations must be obtained to test the predictions of the theoretical calculations at these levels. Measurements of the velocity amplitude versus altitude, of velocity phase differences, and of velocity-intensity phase differences will be needed from simultaneous observations in different spectral lines and with high spectral resolution.

The p-modes should also be searched for in the transition zone with the UVSP instrument onboard the Solar Maximum Mission satellite. This instrument has the ability to make repeatable roster scans with a long, slender entrance slit in much the manner done thus far from the ground.

4.4 Very-High Wavenumber Observations

Observations are needed of the oscillations at spatial wavelengths smaller than 2 arcseconds (i.e. with 1 arcsecond resolution or better) in order to search for vertically-propagating p- and g-modes.

4.5 Search for Lifetimes and Excitation Mechanisms of Modes

Continuous multiday observing runs should help determine the lifetimes of the various modes. Such observing runs should also allow studies to be made of the rate of modal excitation and decay.

5. Needed Theoretical Improvements

As discussed earlier the observations of low-ℓ modes require that all known inaccuracies in the computation of solar models be removed to a level of better than 0.1 percent. The influence of the non-adiabatic terms on the p-mode frequencies must be studied in more detail for low values of ℓ. The sensitivity of the low-ℓ value frequencies to changes in the location and type of outer boundary condition must also be studied.

The calculation of the effective depths of different modes for rotational velocity determinations must be revised and generalized now that the models extend much more deeply into the sun. The approach we have taken thus far (see Ulrich, Rhodes, and Deubner, 1979) may be too conservative in the depth estimates for those modes which extend inward below the base of the convective zone.

The influence of magnetic fields upon the p-mode eigenfrequencies must be tested by the inclusion of magnetic fields in the oscillation equations. Magnetic fields in various strengths and configurations should be modeled both above the photosphere and in the convection zone.

We also need to study any potential nonlinear mode coupling mechanisms which might be operating to limit the amplitudes of the observed modes or to couple the modes to convective motions. And lastly, we need to undertake systematic calculations of radial and non-radial g-modes with the same models we are currently using for the p-modes. We need to determine the horizontal wavenumber structure of the different interior g-modes and calculate the predicted frequencies and wavenumbers of g-modes which might be trapped in chromosphere.

Summarizing, in spite of the rapid progress which has been made in the past five years, much work remains to be undertaken in both the observational and theoretical studies of solar oscillations before we can exploit them to their maximum potential as probes of the solar atmosphere and interior.

Acknowledgements

The observations which were made at the Kitt Peak National Observatory were obtained with the assistance of Richard Aikens and members of the staff of the solar program at Kitt Peak. Some of the reduction of this data was also carried out on the KPNO computing facilities. The Kitt Peak National Observatory is operated by AURA, Inc. for the National Science Foundation. We also wish to acknowledge the assistance of Philip Dumont and George Hawkins of the UCLA Astronomy Department with the theoretical calculations. The assistance of the campus computing centers at both USC and UCLA was also instrumental in the completion of both the observational data reduction and the theoretical calculations. Financial support for this work was provided by the following: the University of Southern California, the University of California at Los Angeles, the National Aeronautics and Space Administration through Grants NSG7407 and NAGW-13, and the National Science Foundation under Grants AST78-20236 and ATM80-09469.

References

Christensen-Dalsgaard, J., Gough, D. O., and Morgan, J. G., 1979, Astron. and Astrophys., 73, 121.

Claverie, A., Isaak, G. R., McLeod, C. P., Van der Raay, H. B., and Roca-Cortes, T., 1979, Nature, 282, 591.

Deubner, F.-L., 1975, Astron. and Astrophys., 44, 371.

Deubner, F.-L., Ulrich, R. K., and Rhodes, E. J., Jr., 1979, Astron. and Astrophys., 72, 177.

Frazier, E. N., 1968, Z. F. Astrophys, 68, 345.

Grec, G., Fossat, E., and Pomerantz, M., 1980, preprint submitted to Nature.

Leighton, R. B., Noyes, R. W., and Simon, G. W., 1962, Ap. J., 135, 474.

Lubow, S. H., Rhodes, E. J., Jr., and Ulrich, R. K., 1980, Lecture Notes in Physics, vol. 25, ed. H. A. Hill and W. A. Dziembowski, Springer-Verlag, Berlin, 300.

Rhodes, E. J., Jr., 1979, in Study of the Solar Cycle from Space, NASA Conference Publication 2098, 159.

Rhodes, E. J., Jr., and Ulrich, R. K., 1980, Bull. A.A.S., 12, 475.

Rhodes, E. J., Jr., Howard, R. F., Ulrich, R. K., and Smith, E. J., 1981, these proceedings.

Rhodes, E. J., Jr., Ulrich, R. K., and Simon, G. W., 1977a, Ap. J., 218, 901.

Rhodes, E. J., Jr., Ulrich, R. K., and Simon, G. W., 1977b, Proceedings of the Nov. 7-10, 1977 OSO-8 Workshop, Univ. Colorado, Boulder, Colo., 365.

Ross, J. E., and Aller, L. H., 1976, Science, 191, 1223.

Ulrich, R. K., 1979, Ap. J., 162, 993.

Ulrich, R. K., and Rhodes, E. J., Jr., 1977, Ap. J., 218, 521.

Ulrich, R. K., Rhodes, E. J., Jr., and Deubner, F.-L., 1979, Ap. J., 227, 638.